Check for updates

Electrochemical Carbon Dioxide Reduction to Ethylene: From Mechanistic Understanding to Catalyst Surface Engineering

Junpeng Qu[1], Xianjun Cao[1], Li Gao[1], Jiayi Li[1], Lu Li[1], Yuhan Xie[2], Yufei Zhao[1] ✉,
Jinqiang Zhang[2,3] ✉, Minghong Wu[1] ✉, Hao Liu[2] ✉

HIGHLIGHTS

- Three key processes in carbon dioxide reduction reaction (CO_2RR) for ethylene generation were discussed, including CO_2 adsorption/activation, *CO intermediates formation, and C-C coupling.

- The preferable mechanism for ethylene over C_1 and other C_2 products reaction pathways.

- Engineering strategies of Cu-based catalysts for CO_2RR-ethylene.

ABSTRACT Electrochemical carbon dioxide reduction reaction (CO_2RR) provides a promising way to convert CO_2 to chemicals. The multicarbon (C_{2+}) products, especially ethylene, are of great interest due to their versatile industrial applications. However, selectively reducing CO_2 to ethylene is still challenging as the additional energy required for the C–C coupling step results in large overpotential and many competing products. Nonetheless, mechanistic understanding of the key steps and preferred reaction pathways/conditions, as well as rational design of novel catalysts for ethylene production have been regarded as promising approaches to achieving the highly efficient and selective CO_2RR. In this review, we first illustrate the key steps for CO_2RR to ethylene (*e.g.*, CO_2 adsorption/activation, formation of *CO intermediate, C–C coupling step), offering mechanistic understanding of CO_2RR conversion to ethylene. Then the alternative reaction pathways and conditions for the formation of ethylene and competitive products (C_1 and other C_{2+} products) are investigated, guiding the further design and development of preferred conditions

for ethylene generation. Engineering strategies of Cu-based catalysts for CO_2RR-ethylene are further summarized, and the correlations of reaction mechanism/pathways, engineering strategies and selectivity are elaborated. Finally, major challenges and perspectives in the research area of CO_2RR are proposed for future development and practical applications.

KEYWORDS Key steps in CO_2RR-ethylene; Preferable reaction pathways; Mechanism understanding; Surface engineering strategies of Cu-based catalysts

Junpeng Qu and Xianjun Cao have contributed equally to this work.

✉ Yufei Zhao, yufei-zhao@shu.edu.cn; Jinqiang Zhang, jinqiang.zhang@utoronto.ca; Minghong Wu, mhwu@shu.edu.cn; Hao Liu, hao.liu@uts.edu.au

[1] Joint International Laboratory on Environmental and Energy Frontier Materials, School of Environmental and Chemical Engineering, Shanghai University, Shanghai 200444, People's Republic of China

[2] Centre for Clean Energy Technology, Faculty of Science, University of Technology Sydney, Broadway, Sydney, NSW 2007, Australia

[3] Department of Electrical and Computer Engineering, University of Toronto, 35 St George Street, Toronto, ON M5S 1A4, Canada

1 Introduction

The widespread usage of fossil fuels has destroyed the balance of the carbon cycle, resulting in a sharp increase in carbon dioxide (CO_2) concentration in the atmosphere, which makes the greenhouse effect an urgent global problem [1–7]. Developing a promising strategy and system to convert CO_2 into value-added products has attracted intensive research interest. However, CO_2 is chemically inert and the activation of CO_2 under ambient conditions is exceptionally challenging [8, 9]. Electrochemical carbon dioxide reduction reaction (CO_2RR), among the approaches for CO_2 conversion, is an attractive route that offers a variety of reduction products coupled by multiple proton transfer steps, ranging from C_1 (e.g., formic acid (HCOOH), carbon monoxide (CO)), C_2 (e.g., acetic acid (CH_3COOH), ethylene (C_2H_4), ethanol (C_2H_5OH,)), C_3 (e.g., acetone (CH_3COCH_3), propanol (C_3H_7OH)), and beyond (e.g., n-butane (C_4H_{10})) [10–13]. In particular, closing the anthropogenic carbon cycle and establishing a sustainable carbon economy are made possible by CO_2 electrolysis, which is powered by electricity generated from renewable energy sources [14, 15].

Compared to other products, reducing CO_2 to ethylene is more desirable due to its larger market necessity and has the highest value among all reduction products [16]. For instance, ethylene is the basic raw chemical material for the polymer industry, pharmaceuticals and high-tech material synthesis. In addition, ethylene can be utilized directly as welding fuels or natural gas additives. Currently, ethylene is mainly manufactured by cracking non-renewable naphtha at high temperatures. The production process is energy-consuming and usually has a negative impact on the environment. Conversely, CO_2RR is an alternative way that is green and sustainable to selectively produce ethylene. Currently, the crucial challenge for converting CO_2 to ethylene electrochemically is to promote the C–C bond coupling while suppressing the competing reactions such as alternative product formation and hydrogen generation. Cu-based catalysts have been proven to exhibit the best capability for producing ethylene. However, they still suffer from low Faraday efficiency (FE) and poor selectivity. Therefore, it is essential to design novel catalysts for highly efficient CO_2 conversion to ethylene [17].

The reaction pathways and reactivity of CO_2RR are heavily reliant on the surface properties and the local reaction environment of catalysts. Slightly alternation of the electrode-electrolyte interfaces may significantly influence the catalytic capability and thus tune the overall catalytic performance [18, 19]. Thus, the sensible design of novel Cu-based catalysts with the geometric effect and electronic effect have been regarded as promising ways to increase the adsorption and desorption energies of the ethylene intermediates, which could lead to high selectivity to ethylene [20–24]. A variety of strategies have been adopted to selectively produce ethylene, including nanostructures control [25–29], defects engineering [30, 31], surface modification [14, 32, 33], and oxidation state alteration [34]. These engineering strategies possess unique mechanisms to promote ethylene production. For instance, altering Cu nanostructures (e.g., constructing unique dendrite structures) can efficiently increase the catalytic active sites and the local pH, benefiting ethylene generation [35]. It is also a common and effective strategy to control the crystal facets and phases to alter the binding energy of intermediates which are also beneficial to the formation of ethylene. Defects can contribute to more active sites, regulate electron distribution, and reduce the energy barrier of C–C coupling. Surface modification by coating molecules (e.g., polytetrafluoroethylene) on Cu surface forms a hydrophobic layer, efficiently restraining the competitive hydrogen evolution reaction (HER) and boosting the C_2H_4 yield [36, 37]. Furthermore, Cu^+ can improve the binding ability of *CO, thus promoting *CO interaction and dimerization [38]. Therefore, engineering Cu-based catalysts to achieve maximized active sites, optimized energy barrier of *CO dimerization, and increased local pH, is essential for selectively producing ethylene.

Although several review articles have summarized Cu-based catalysts for CO_2RR to produce C_{2+} products, little attention has been drawn to specifically and systematically discussing the engineering effects of novel Cu-based catalysts for ethylene production. In this review, we focus on the key influences on the production of C_2H_4, and various engineering strategies on Cu-based catalysts to selectively reduce CO_2 into C_2H_4. We firstly summarize the production mechanisms by reviewing the important steps for CO_2RR to ethylene, including the CO_2 adsorption/activation, formation of *CO intermediate, the key C–C coupling step for ethylene formation, to provide an overview understanding of the fundamental principles of CO_2RR process. Then, we investigate differences in the reaction pathways and conditions for the formation of ethylene and competitive products (C_1 and

other C_{2+}), providing a specific guideline to design efficient electrocatalysts. We further discuss the design and engineering strategies of Cu-based catalysts for CO_2RR conversion to ethylene based on altering the composition, structure, surface state, etc. In particular, the reaction mechanism and correlations between the engineering strategies and selectivity towards ethylene are specifically focused on. Finally, the challenges and perspectives for CO_2RR are outlined and discussed.

2 Fundamental and Mechanism of CO_2RR to Ethylene

Generally, the electrochemical CO_2RR occurs at the three-phase interface, including the gaseous reactant CO_2, liquid electrolyte and solid catalysts. The CO_2RR process is very complicated due to the presence of many possible intermediates/products with altering the proton-electron transfer, multiple electron transfer and reaction pathways [5]. Specifically, the CO_2 conversion reaction to ethylene requires a 12-electron transfer with proton coupling, which involves multiple possible intermediates such as *COCHO, *CH*COH, *OCHCH*O and CH_2CH*O [5, 39–42]. The formation and reaction pathways of these intermediates can be affected by many parameters, such as the electrolyte compositions, applied potentials, temperatures, pH, etc. Therefore, understanding the reaction pathways to selectively generate ethylene is critical for guiding the catalyst design to achieve excellent electrochemical performance. Thus in this section, we will discuss three key processes in CO_2RR for ethylene generation: CO_2 adsorption/activation, *CO intermediates formation, and C–C coupling (Fig. 1).

2.1 CO_2 Adsorption/Activation

The adsorption and activation of CO_2 on the active sites in CO_2RR process are essential for the subsequent reduction process, as optimal energy level can suppress the competing reaction HER [43–46]. Generally, there are two CO_2 adsorption states on the catalysts. One is to form linear molecules through physical adsorption, and the other is to form charged $CO_2^{\delta\cdot-}$ species through chemical adsorption (Fig. 2a) [45, 47, 48]. A $CO_2^{\delta\cdot-}$ intermediate is usually generated on the catalysts with C atom as the bonding site, when only electrons are involved in the activation process. Alternatively,
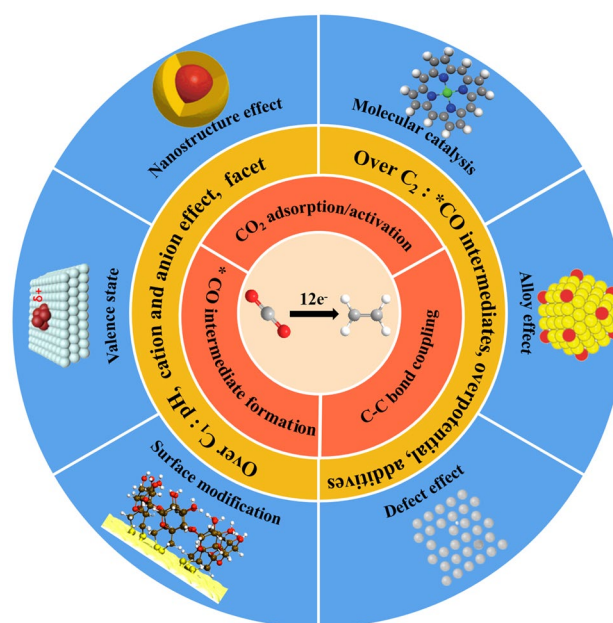
Fig. 1 Overview of this review. Three key processes in CO_2RR for ethylene generation. The preferable mechanism for ethylene over C_1 and other C_{2+} products reaction pathways. And strategies for designing Cu-based catalysts for CO_2RR to ethylene

when both protons and electrons participate in the CO_2 adsorption/activation process, *COOH is the intermediate with C as binding atoms, followed by the hydroxyl removal and *CO formation, which can be further converted into a number of products, including C_1 (CH_4, CH_3OH, CO) and C_{2+} products (C_2H_5OH, C_2H_4, CH_3COOH, C_3H_7OH). In contrast, *OCOH intermediates are formed if O atoms act as bonding atoms instead of C, which later are only converted to HCOOH (Fig. 2b) [49].

2.2 *CO Intermediate Formation

The adsorption and activation process generates intermediates that are important for the subsequent reduction reactions. The most important intermediate is *CO which is generated from the as-formed *COOH intermediate by proton coupling electron transfer (PCET) process to remove a molecule of H_2O. The *CO species can be directly desorbed from the catalysts (e.g., Ag and Au) when *CO adsorption energy is low, forming CO gas (the mechanism of electrochemical CO_2RR to form CO) (Fig. 2c) [49, 50]. Alternatively, moderate *CO adsorption energy (e.g., Cu) can lead to further coupling and
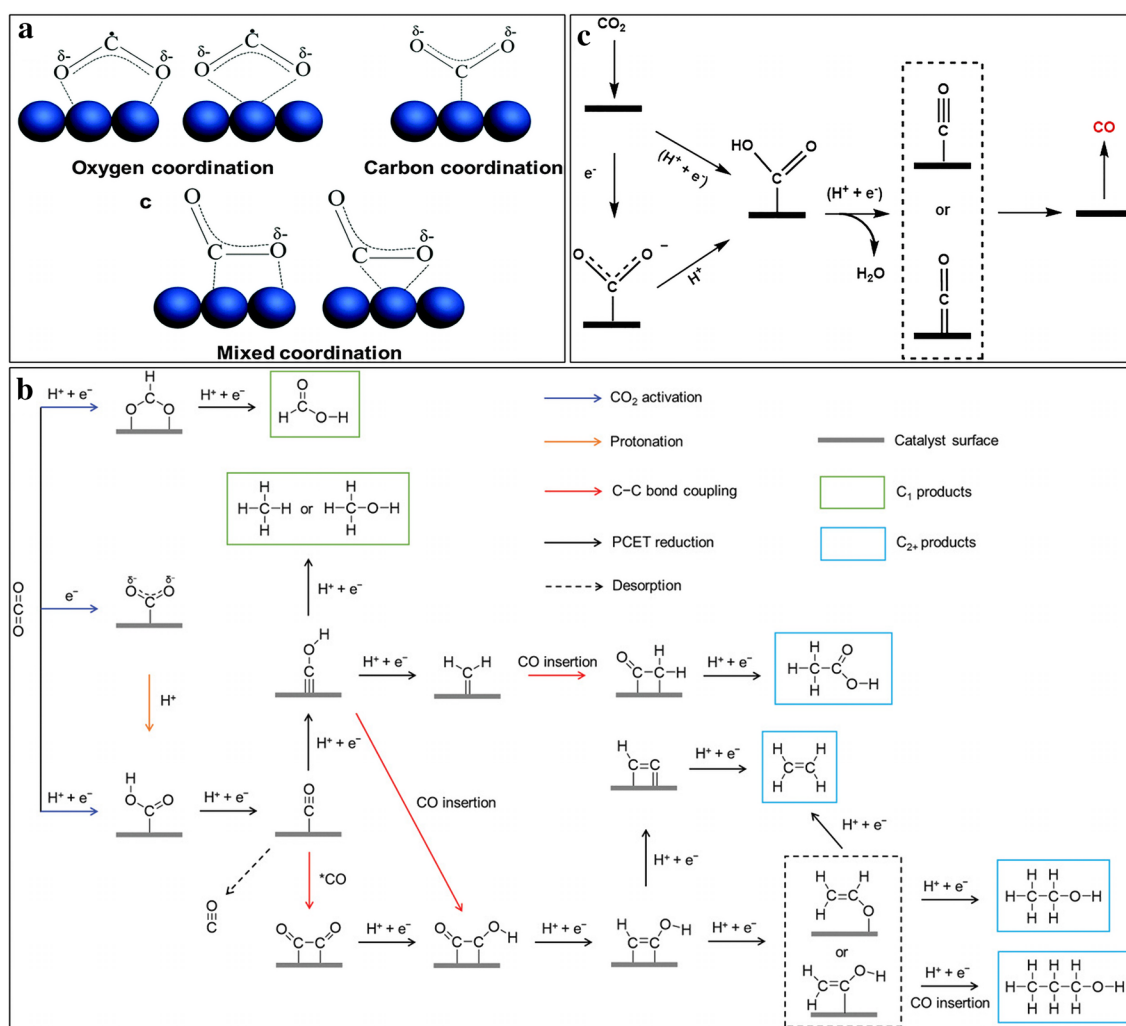
Fig. 2 **a** The potential structures of adsorbed $CO_2^{\delta\cdot-}$ on catalysts surface [47]. Reused with approval; Copyright 2008 Royal Society of Chemistry. **b** Potential structure of CO_2 activation and reaction route of generation to various products. **c** Potential reaction route for electroreduction of CO_2 to CO [49]. Reused with approval; Copyright 2017 Elsevier

formation of C–C bonds for promoting the following C_{2+} production, based on the Sabatier principle [40]. Furthermore, *CO coverage is also crucial for CO_2-to-C_{2+}, as high coverage of *CO occupies most of the catalytic active sites can not only reduce the hydrogen adsorption and suppress HER, but also increase the chance of C–C coupling, boosting CO_2 to C_{2+} conversion efficiency [51]. However, it is noteworthy that increasing *CO coverage reduces the affinity of C atoms on Cu surface, which is beneficial to generate oxygenates (especially acetate) rather than ethylene [52]. Therefore, balancing the *CO coverage on the designed catalysts is vital to produce ethylene in CO_2RR process.

2.3 C–C Bond Coupling

C–C bond coupling is one of the essential steps in the CO_2RR process to generate C_{2+} products such as ethylene. Three routes for C–C bond coupling have been proposed for the generation of C_{2+} products (Fig. 3).

The first route is the direct dimerization of the adsorbed *CO intermediates resulting in *CO*CO intermediate through C–C coupling [53]. With the aid of proton coupling and electron transfer, the *CO*CO species are further converted into *CO*COH intermediates on Cu(100) [54]. The presence of OH group in *CO*COH intermediates breaks the charge distribution balance from the symmetrical structure of *CO*CO intermediate, which may lead to the appearance
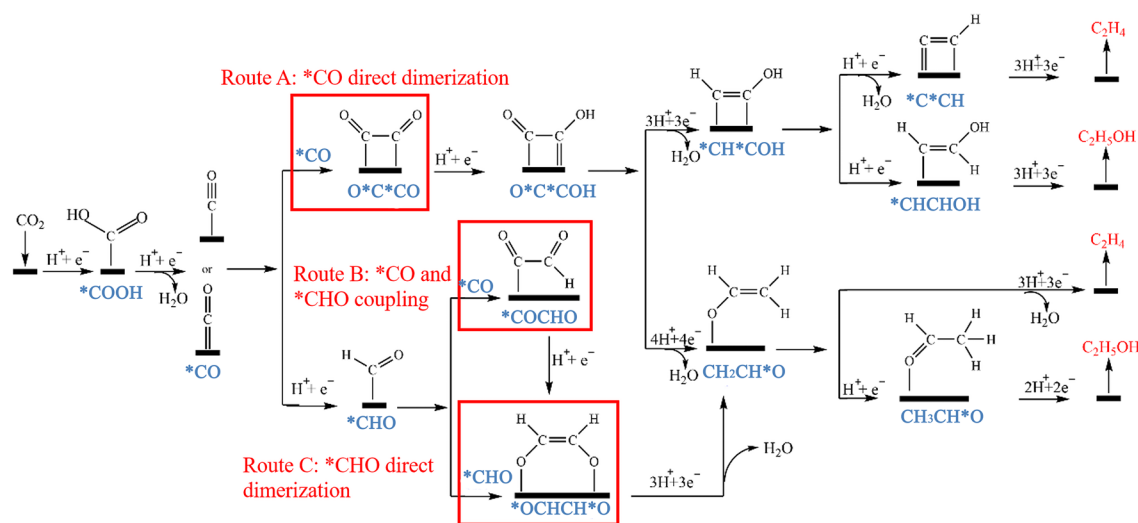
Fig. 3 Potential reaction routes for the electroreduction of CO_2 to ethylene and alcohol [55]. Reused with approval; Copyright 2021 Royal Society of Chemistry

of two different reaction intermediates, *CH*COH or CH$_2$CH*O, when interactions with protons and electrons. The hydrogenolysis of CH$_2$CH*O species produces C$_2$H$_4$, whereas the hydrogenation of CH$_2$CH*O leads to the production of CH$_3$CH*O, resulting in the formation of C$_2$H$_5$OH [55]. The energy barrier of generating C$_2$H$_4$ by CH$_2$CH*O is 0.2 eV lower than that of generating C$_2$H$_5$OH by CH$_3$CH*O [42]. This may be the reason that ethylene is generally more favourable over ethanol on copper-based catalysts. Alternatively, Goddard III and co-workers believed that *CH*COH species is the key intermediate to produce C$_2$H$_4$ and C$_2$H$_5$OH, *CH*COH loses OH group to form *C*CH which is then hydrogenated to form C$_2$H$_4$, whereas, *CH*COH directly hydrogenated to form *CHCHOH which is then hydrogenated to produce C$_2$H$_5$OH [56].

The second possible reaction route is the direct coupling of *CO intermediates with protons to generate *CHO intermediates, which are preferred on Cu(100) surface at high potential or Cu(111) in the full potential range [40, 57]. The dimerization coupling occurs between *CHO and *CO intermediates to form *COCHO species. Due to the hydrogen electrode model, the adsorption energy of *COCHO is 0.16 eV higher than that of *COCOH in the first route, demonstrating the superior stability of *COCHO intermediates. Therefore, compared with the *COCOH intermediate, *COCHO is a more preferred intermediate by the coupling reaction between *CO and *CHO intermediates [40]. The *COCHO is further

hydrogenated to form *OCHCH*O and CH$_2$CH*O, which eventually produces ethylene [41, 56, 58].

The third C–C coupling reaction route relies on the dimerization between *CHO intermediates to form the *OCHCH*O species, which is then converted to CH$_2$CH*O via H$_2$O removal through PCET process, and eventually leads to the ethylene production [39]. It is reported that the dimerization of *CHO intermediate to form C–C bond has more kinetic advantages [59]. For example, the theoretical calculation indicated the energy barrier (0.28 eV) for the formation of C–C bond through *CHO dimerization was much lower than that of the dimerization between *CO and *CHO (1.08 eV) on Cu^0-Cu$^+$atomic interface, indicating that *CHO intermediates were more prone for direct dimerization [60]. In addition, *CO intermediates form C–C bonds directly through dimerization showed a large reaction energy barrier (1.52 eV), thus *CO is preferentially reduced to *COH or *CHO intermediates for further dimerization to produce ethylene [55].

3 Alternative Reaction Pathways and Conditions for the Formation of Ethylene and Competitive Products

Although we have established the most preferable theoretical reaction pathways for CO$_2$RR to produce ethylene in the previous section, experimentally achieving these reaction

pathways remains a great challenge. So far, there have been many factors that can tune the selectivity towards ethylene over the other competing products, such as the microenvironment at the three-phase interface, properties of the catalyst surface and operating conditions, including local pH, cation and anion, surface adsorption substances, catalyst facet, applied overpotential. These physical and/or chemical factors have a vital effect on the thermodynamic adsorption energy of the key intermediates generated in the CO_2RR process, resulting in the alteration of the reaction pathways [40, 41, 61–70]. In this section, we will discuss the alternative reaction pathways and conditions for the formation of ethylene and competitive products (C_1 and other C_{2+} products) systematically.

Generally, the morphology of the catalyst surface, hydrophobicity and adsorption of intermediates can lead to the formation of different products. Similarly, the relevant properties of electrolytes, such as pH, CO_2 solubility and conductivity, can also determine the catalytic performance and selectivity of CO_2RR, due to their direct contact with the active center. Therefore, in order to tune the reduction product towards ethylene, it is essential to explore the effects of different limiting factors for the alteration of product formation. This section summarizes main aspects based on electrolytes, including the effects of pH, anions, cations and additives, as well as the effects of catalyst surface potential and crystal surface.

3.1 Preferable Mechanism for Ethylene over C_1 Products Reaction Pathways

The determinative reaction pathway for the generation of ethylene and C_1 products is the C–C coupling step. The formation of C_1 products generally comes from the low adsorption energy of the C_1 intermediates, which cannot stay longer for C–C coupling on the surface catalysts. For instance, the *CO intermediate can be directly desorbed from the catalysts to evolve CO if the adsorption energy of *CO is low. And the *OCOH intermediate generated on the catalysts can be directly reduced to HCOOH through the PCET step. The adsorption energy of intermediates and adsorption sites of intermediates can be altered by many parameters, such as the pH, cation/anion and facet of catalysts, which will

significantly influence the reaction pathways to produce ethylene over C_1 products.

3.1.1 pH Effect for Ethylene Over C_1

Protons in the electrolyte, especially at the interface between electrode and electrolyte, have a significant effect on the selectivity of reduction products in electrochemical CO_2RR. When the pH at the interface is low, the C_1 pathway is the main thermodynamic reaction route [58, 71, 72], e.g., the formation of CH_4 from the *COH intermediate by *CO hydrogenation [73–76]. At high pH, the dimerization of *C_1 intermediates (*CO and *COH) is the dominant reaction both thermodynamically and kinetically, whereas the C_1 pathway is inhibited due to a higher reaction energy barrier, leading to the production of C_2 products preferably C_2H_4 (Fig. 4a). Under neutral conditions, on the other hand, C_1 intermediates may not proceed through both C_1 and C_2 pathways, but could generate multi-carbon products owing to the cross-coupling of these intermediates (e.g., *COH with *CO) [77]. The water molecules binding to the surface of the Cu catalysts play an indispensable role in selectively generating hydrocarbons or oxygenates. Specifically, the surface-adsorbed H_2O is usually the proton source in the reaction, directly combining *H with the OH group of the adsorbed intermediates, and then removing a molecule of water, thereby promoting the production of hydrocarbons like ethylene. It is worth mentioning that not just the pH of the bulk electrolyte (such as KCl and $KHCO_3$) can affect the product distribution. The local pH change at the interface during the CO_2RR process can also change the selectivity. It has been demonstrated that in electrolytes with weak buffering capacity such as KCl, $KClO_4$ and K_2SO_4, H^+ is continuously consumed and the local pH on the electrode surface increases as the reduction reaction progresses, which is favourable for the production of ethylene [78, 79].

Remarkably, the pH value also affects the competitive HER. CO_2RR and HER occur simultaneously in the aqueous electrolyte, since the redox potential of the proton to H_2 is very close to the redox potential of CO_2 conversion, leading to a significant drop of the FE of ethylene [80]. Generally, the production of H_2 is achieved via the direct reduction of protons in the electrolyte ($2H^+ + 2e^- \rightarrow H_2$) or the reduction of the solvent ($2H_2O + 2e^- \rightarrow H_2 + 2OH^-$), indicating a low pH is preferred for HER [81]. Therefore,
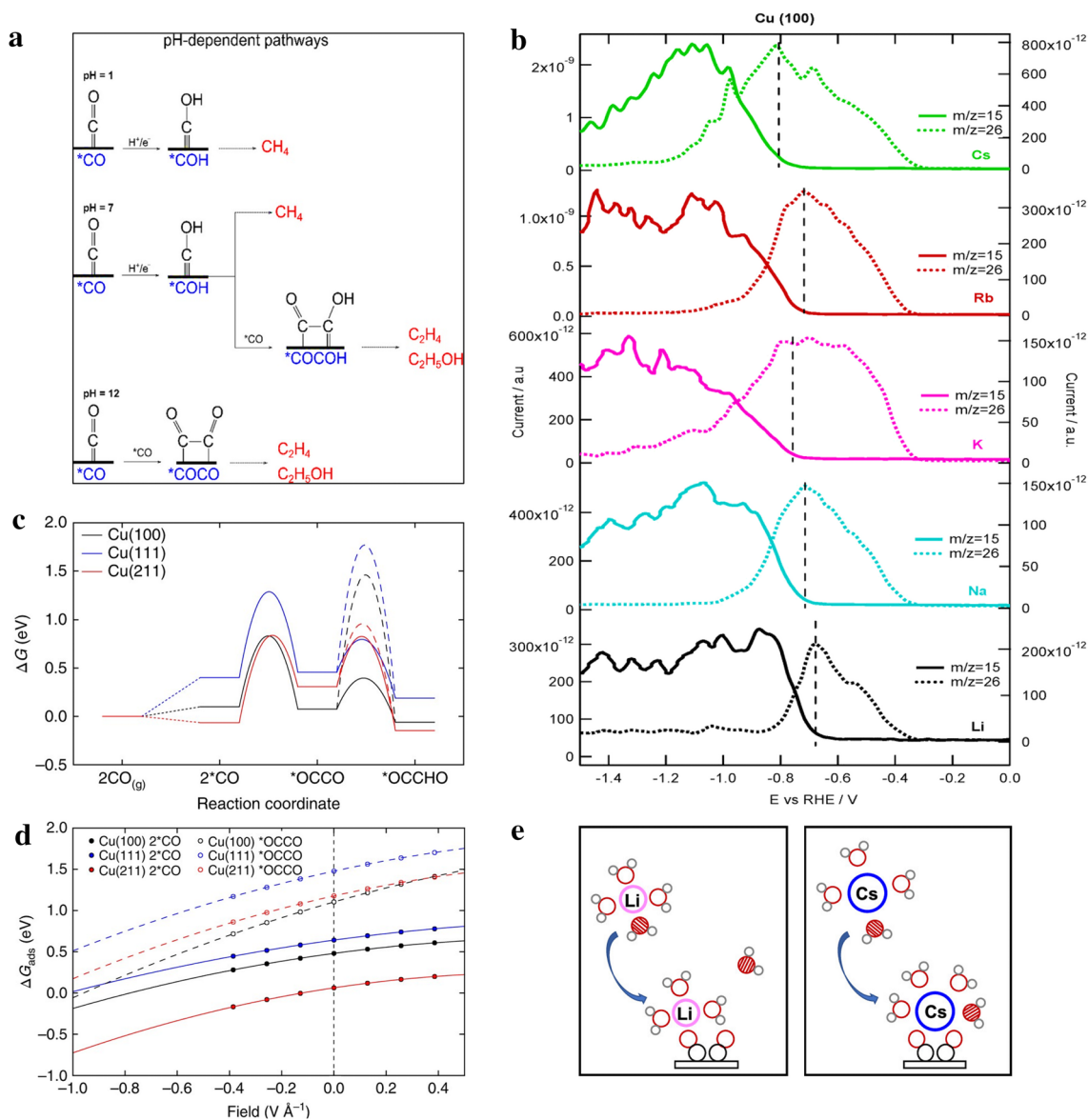
Fig. 4 **a** The pH-dependent reaction routes for CH_4 and C_2H_4 on the Cu(111) surface [77]. Reused with approval; Copyright 2016 American Chemical Society. **b** OLEMS signals of CO reduction products in 0.1 M hydroxide solution with different cations. The dotted line corresponds to ethylene, and the solid line corresponds to methane [87]. Reused with approval; Copyright 2017 American Chemical Society. **c** *CO is directly dimerized into the free energy diagram of *CO*CO, the surface hydrogenation is represented by the dotted line and the proton-electron transfer is represented by the solid line form the free energy diagram of *OCCHO, at 0 V vs. RHE. **d** Binding free energy of *CO and *CO*CO on different facets [99]. Reused with approval; Copyright 2018 Springer Nature. **e** Diagram of dynamic coordination between alkali metal ions (Li^+ and Cs^+), intermediates and water on CO_2RR [90]. Reused with approval; Copyright 2021 American Chemical Society

it is necessary to increase the pH value of the electrolyte in order to improve the CO_2RR while suppressing HER. Furthermore, as high pH is also considered beneficial for C_{2+} production, most studies have been carried out in neutral or alkaline electrolytes [82]. Similarly, designing and controlling the morphology of the electrocatalysts which can increase the local pH value during the reaction is also an excellent strategy to improve the CO_2 reduction products, such as developing nanowire arrays, dendritic structures, etc. [35, 83]. This will be illustrated in detail in the catalyst design section.

3.1.2 Cation and Anion Effect

The change of type or concentration of cations in the electrolyte can significantly affect the activity of CO_2RR and the selectivity towards the targeted products [78, 84–86]. Cations at the interface can change the microenvironment or interact with the intermediates, which act as promoters in CO_2RR by changing the free energy pattern and stabilizing specific intermediates. Generally, smaller cations with higher charges are prone to attract more water molecules to form a larger hydration layer, leading to the increase of H^+. Cations with smaller hydration layers (such as Cs^+) can get closer to the surface of catalysts and enrich the outer Helmholtz layer, making the interface electric field stronger (Fig. 4b) [87]. The strong dipole interactions between the stronger interface electric field and the surface adsorbate promote the proceeding of CO_2RR. Meanwhile, solvated cations induced by interfacial electric field can also stabilize CO_2 and intermediates with different dipole moments through electrostatic interaction. The enrichment of alkali metal cations (such as Cs^+ and K^+) in the outer Helmholtz layer can also decrease the activity of competing HER, due to the steric hindrance effect of larger cations to H^+ on the outer Helmholtz layer [88]. Therefore, larger cations (such as Cs^+) are more effective in promoting the reaction pathway of the intermediates to selectively produce C_{2+} products, especially ethylene, compared to smaller cations (such as Li^+) [89]. Furthermore, *CO intermediates have been demonstrated to function as the ligand for cations, which may promote the formation of C–C bond of *CO intermediate, as larger cations have a much higher chance to attract more *CO (Fig. 4e) [90]. Thus, the as-formed cation-intermediate complex is crucial to promote the formation of C_{2+} products. Furthermore, as the radius of alkali metal cations increases from Li^+, K^+ to Cs^+, the free energy barrier of *CO dimerization decreases gradually according to the DFT calculations [91]. The presence of larger cations is also beneficial to the formation of other C_2 and C_3 products (such as acetic acid, glycolic acid, ethanol and propanol) owing to the negative potential required for forming *OCCOH from *CO in the presence of Cs^+ compared to Li^+ or Na^+.

In addition to changing the local electric field and stabilizing the reaction intermediate, the hydrated alkali metal cation in the electrolyte can also affect the local pH of the buffer interface [92–94]. The hydrated alkali metal cation will be subjected to the electrostatic interaction of the applied voltage on the cathode, thereby reducing the pK_a of the hydrolysis [92]. The larger size of the alkali metal cation, the greater the electrostatic effect, leading to smaller pK_a. The hydrolysis reaction is a dynamic equilibrium process [94]. When the pK_a of the hydrated alkali metal cation is lower than the local pH value of the interface, it will promote the production of H^+ in the electrolyte buffering the local pH value. This will further alleviate the polarization and Nernst loss caused by the increase of local pH under CO_2RR conditions and ultimately promote the conversion of CO_2 instead of H_2 [95].

The anion effect has been also investigated for CO_2RR process. Both anions with buffering capacity (bicarbonate (HCO_3^-), borate ($H_3BO_3^-$), phosphate (HPO_4^{2-})) and anions without buffering capacity (perchlorate (ClO_4^-), sulphate (SO_4^{2-})) have been studied for their influence on the product distribution in CO_2RR. The results revealed that electrolytes with stronger buffering capacity can contribute protons more effectively, thus are prone to produce H_2 and CH_4 while inhibiting the generation of CO, HCOOH, C_2H_4 and C_2H_5OH, etc. [21, 96, 97]. Therefore, it is preferred to have electrolytes with lower buffer capacity to generate C_2H_4 as the main reduction products over C_1 chemicals and H_2.

3.1.3 Facet Effect for Ethylene over C_1

It has been demonstrated that the selectivity of CO_2RR process showed a strong dependence on crystal planes of Cu. For example, C_2H_4 is prone to be formed on Cu(100), while Cu(111) is favourable for the formation of C_1 products (CH_4 and $HCOO^-$) [98]. The atomic configuration on the surface of Cu(100) provides the best adsorption geometry for the *CO dimers and stabilises the charged intermediates (*CO*CO) for C_2H_4 generation (Fig. 4c, d) [99, 100]. For instance, nanostructured Cu films with more exposed Cu(100) facet could effectively increase the *CO coverage and reduce the C–C coupling energy barrier, achieving FE_{C2H4} of 58.6% at − 0.75 V vs. RHE [46]. However, by adding Cu^{2+} to the electrolyte to passivate the Cu nanosheet (NSs), the dissolution of the Cu NSs was inhibited and the exposed Cu(111) surface was maintained, leading to the selectivity of CH_4 with 70% FE at − 1.6 V vs. RHE [101]. The instrument characterization results show that Cu(111) surface was prone to produce intermediates such as *COOH and *CH_2O, which are favourable to forming CH_4.

3.2 Preferable Mechanism for Ethylene Over Other C$_{2+}$ Products Reaction Pathways

Generally, all C$_{2+}$ products are obtained after C–C coupling step. Therefore, they may share similar reaction intermediates during the reduction processes. Thus, compared to C$_1$ vs. ethylene, it is relatively difficult to tune the selectivity between these C$_{2+}$ products. However, it is possible to change the conversion tendency of these shared reactions intermediates to different directions by applying different influencing factors, leading to the formation of different reduction products. For instance, ethylene production can be improved by converting *CH*COH to *C*CH by controlling the content of *CO intermediates. In this section, we mainly discuss the influence of *CO intermediates, overpotential and additives on the reaction pathways of ethylene over other C$_{2+}$ products.

3.2.1 *CO Intermediates Effect

Since *CO intermediates are the keys for C–C coupling to produce C$_{2+}$ products, it is necessary to understand the relationship between *CO intermediates and the formation pathways of ethylene and the competitive products. As shown in Fig. 5a, the *CH*COH (denoted IM) intermediate is the bifurcation point of the ethanol and ethylene reaction pathways [41, 56, 58]. Thus, it is desirable to control the reaction direction from IM to *C*CH (denoted IM-C) while inhibiting the *CHCHOH (denoted IM-O) pathway to promote ethylene production [102]. The theoretical investigation of the reaction energies of IM-C and IM-O pathways unravelled that the lower coverage of *CO on the catalyst's surface diminished the enthalpy change of the IM-C pathway, benefiting ethylene production rather than ethanol. However, higher *CO coverage is beneficial to the C–C bond coupling and lower free energy barriers of both the IM-C and IM-O pathways, boosting the overall CO$_2$RR process to C$_{2+}$ products (Fig. 5b). Therefore, it is vital to maintain proper *CO coverage achieve maximal ethylene selectivity (Fig. 5c) [102]. Intermediates from *CO can also influence the formation of different products. It has shown that *CHO from *CO hydrogenation is a common intermediate for C$_{2+}$ products on Cu. By coupling with another *CO, it can convert to *COCHO, which forms CH*CO through hydrogenation and dehydroxylation [52]. It has been proposed by Abild

Pedersen and his colleagues the hydrogenation of CH*CO is the branch point between ethylene and oxygenates. Theoretical calculation results demonstrated that the repulsive interaction between *CO tends to generate oxygenates, due to increasing *CO pressure has to decrease the surface water adsorption, resulting in the low content of protons. Therefore, the increase of *CO coverage is beneficial to the selectivity of oxygenates (especially acetate, requiring a minimum of protons), rather than ethylene (Fig. 5d) [52].

3.2.2 Overpotential Effect

The applied overpotential can also influence the CO$_2$RR selectivity to produce specific C$_{2+}$ products by altering the stability of intermediates [42, 56]. For instance, *CO*CO prefer to form under low potential, whereas high potential results in the formation of *COCHO (Fig. 5h) [57, 58, 98]. Specifically, on the Cu(100) surface, when the overpotential is higher than -0.6 V, C–C coupling preferentially proceeds through the *CO*CO pathway, followed by forming *COCHO, leading to the generation of C$_2$H$_4$ with a lower energy barrier of 0.69 eV. When the overpotential is at the range of -0.6 to -0.8 V, *H and *CO share similar adsorption energy, leading to low *CO coverage at the active sites and higher HER. When the overpotential is more negative than -0.8 V, *COCHO is formed by coupling *CHO with non-adsorbed CO, leading to the formation of C$_2$H$_4$ and CH$_4$ depending on the mass transfer rate of non-adsorbed CO [96, 103]. The theoretical calculations demonstrated that when the overpotential was higher than -0.6 V, ethylene was the main hydrocarbon product due to the low energy barrier of 0.69 eV for two *CO couples to form a C–C bond [56].

3.2.3 Additives Effect for Ethylene over C$_2$

Incorporating additives in electrolytes affects the microenvironment at the interface of catalysts/electrolytes, which changes the corresponding properties of local electrolytes, such as pH, hydrophobic layer, conductivity, solubility and viscosity. These properties will have a significant effect on the CO$_2$RR catalytic performance and selectivity (Fig. 5i) [104–106]. It has been demonstrated that the hydrophilic interface generally promotes the formation of *COOH (then formic acid), while the hydrophobic interface is conducive to the generation of
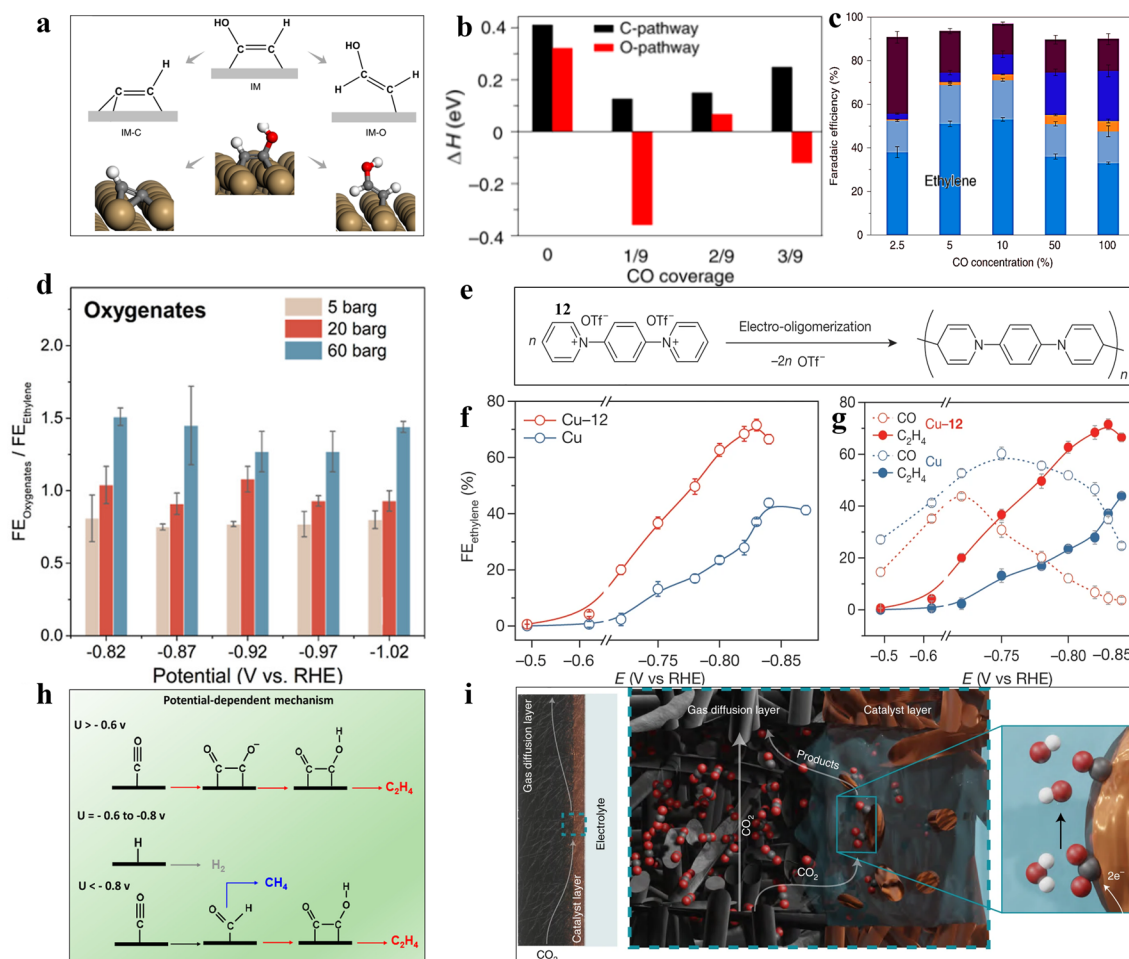
Fig. 5 DFT-calculated effects of *CO coverage on selectivity between ethylene and alcohols. **a** A schematic plot of the reaction mechanism where the last oxygen-containing group in *CHCHOH (IM) is removed, forming *CCH (IM-C), and an alternative route to *CHCHOH (IM-O), as well as the geometries of IM, IM-C and IM-O on Cu(100) surfaces. **b** Enthalpy changes for the IM-C and IM-O routes at different levels of *CO coverage. **c** FEs of CORR products at various *CO concentrations at − 0.44 V vs. RHE in 1 M KOH [102]. Reused with approval; Copyright 2019 Springer Nature. **d** Pressure-dependent of $FE_{oxygenates}/FE_{ethylene}$ at different potentials and pressures on polycrystalline Cu in 0.1 M phosphate buffer with pH = 8 [52]. Reused with approval; Copyright 2022 American Chemical Society. **e** Schematic diagram of N,N'-(1,4-phenylene)bispyridinium salt 12 to form an N-aryl-dihydropyridine-based oligomer. **f** FE of ethylene on Cu and Cu-12. **g** FEs of CO and ethylene on Cu and Cu-12 at − 0.47 V to − 0.84 V vs. RHE [14]. Reused with approval; Copyright 2020 Springer Nature. **h** Potential-dependent reaction routes for CH_4 and C_2H_4 on the Cu(100) surface [98]. Reused with approval; Copyright 2019 American Chemical Society. **i** Surface-interface microenvironment of gas diffusion electrode in CO_2 electrolysis [104]. Reused with approval; Copyright 2022 Springer Nature

*CO. The surface hydrophobicity property can also limit the proton and water transport, thus forming a locally high pH at the interface, inhibiting the competitive HER [107]. It also possesses the advantage to reduce the thickness of CO_2 diffusion layer, forming a highly active and stable three-phase interface microenvironment. For example, 1-octadecanethiol was added to the surface of dendritic Cu for catalyst surface modification [32]. Due to the presence of long carbon chains, the contact angle between the Cu surface and the electrolyte increased sharply from

17° to 153°. The improvement of hydrophobicity is more conducive to the capture and release of gas reactants and products at the three-phase interface while inhibiting the competitive reaction (HER). As a result, highly selective production of ethylene was achieved with FE_{C2H4} = 56% at − 1.5 V vs. RHE. Another example is the use of organic molecule (N,N'-(1,4-phenylene)bispyridinium-derived oligomer) to modify the Cu surface (Fig. 5e–g) [14]. The N bader charge in organic molecule affects the production of $*CO_{atop}$, which is more conducive to C–C

coupling kinetically. Spectroscopic characterization and simulation calculations showed that the organic molecule adhered to the catalyst surface improved the stability of $*CO_{atop}$, which promote the selectivity to ethylene (FE of 72% at $-0.83V$ vs. RHE).

4 Engineering Strategies of Efficient Catalysts for Electrocatalytic CO_2RR to Ethylene

So far, the most efficient catalysts in CO_2RR to produce ethylene are the Cu-based electrocatalysts. However, the pristine Cu catalysts suffer from the insufficient selectivity to ethylene and low overall FE of carbon-based products. There are many strategies proposed to tune the selectivity of Cu catalysts to produce ethylene [108]. For instance, nanoscale Cu catalysts with high porosity and surface areas are beneficial to the microenvironment optimization (e.g., local pH) and reactants/products diffusion [109]. Applying tandem catalyst systems by designing alloys or molecule-Cu catalysts can tune the surface coverage of *CO intermediate, thus optimizing the selectivity for ethylene generation. Moreover, electronic structure tuning is efficient in altering the intrinsic adsorption capability of reactants/intermediates on the catalysts. Heteroatom doping, e.g., alloys/bimetallic catalysts, have been widely investigated to modulate the electronic structure for high ethylene selectivity. Moreover, specific facet exposure may also serve as an efficient approach to regulate the adsorption of intermediates to generate ethylene. Therefore, efficient engineering strategies such as nanostructure control, molecular catalysis, alloy, defects, surface modification, valence state, etc., can be designed for Cu-based catalysts to selectively enhance the ethylene generation rate while inhibiting the competitive products (H_2, C_1 and other C_{2+}). In this section, we will review various design strategies for Cu-based catalysts, and further investigate the correlation among these strategies, induced specific effects and selectivity for highly efficient producing ethylene.

4.1 Nanostructure Effect

The nanostructure of the designed Cu-based catalysts, including morphology, size, crystal facet, crystal phase, etc., have great influences on the catalytic activity and selectivity of CO_2RR towards ethylene generation. Changing the morphology of catalysts may alter the local pH or reactants concentration near the electrodes. The porous structure is also favourable for the mass transportation of the reactants/intermediates/products. Tuning the exposed facets of the designed catalysts is efficient in regulating the binding strength of intermediates, thus changing the CO_2RR catalytic activity and selectivity. The size of electrocatalysts affects the number of coordination sites. Therefore, regulating the nanostructure of electrocatalysts is significant for the CO_2RR catalytic performance.

4.1.1 Morphology Effect

The designed catalysts with specific morphology may directly influence the reaction mechanism and pathways of CO_2RR, by altering the adsorption energy of intermediates, which results in different selectivity of products [110–114]. For instance, the vertical nanosheet arrays with uniform distribution of Cu catalysts can improve the CO_2RR efficiency to ethylene by accelerating the mass transfer of CO_2 in the electrolyte and near the catalyst surface. Dendrites with cavities/tips/needles can efficiently inhibit the competition of HER by increasing pH in the local environment. Cu catalysts with rough surfaces possess larger specific surface areas, increasing the number of active sites for CO_2 adsorption and activation.

Currently, several morphologies of Cu-based catalysts have been proposed and prepared towards CO_2RR, including nanoparticles, nanocubes, core-shell structures, nanowires, nanoarrays and nanofoam [83, 115–119]. Specifically, nanoarrays and nanocubes can efficiently promote the selective formation of C_2H_4 due to the induced tip effect and changed local pH on the catalyst surface. For example, Cu nanowire arrays have been prepared by electrochemical reduction of CuO nanowire arrays on Cu foil [83]. The derived nanowire arrays with long and dense structures limited the diffusion of the generated OH^- at the surface of electrodes [21, 120], which led to the increase of local pH at the interface of electrode/electrolyte. The designed nanoarrays could efficiently inhibit the production of CH_4 and H_2, and facilitate the selectivity of C_{2+} products, especially C_2H_4. Another example is the Cu nanowires with step surface derived

from activating the Cu nanowires at -1.05 V vs. RHE, which also delivered excellent selectivity towards C_2H_4 (Fig. 6a, b) [27]. Theoretical calculation results demonstrated that the adsorption energy barrier of *CO intermediates on two adjacent active sites of the Cu step surface was much lower than that on Cu(100) [121]. The superior thermodynamic stability and lower C–C coupling barrier of the C_2 path on the step sites led to the maximum FE_{C2H4} = 77.4% at -1.0 V vs. RHE (Fig. 6c). Other than the nanowire structure, the cubic nanoparticles with branches can also promote the selectivity for C_2H_4 generation. For instance, the cubic Cu_2O nanoparticles with branched CuO (B-CuO) were derived by controlling the oxidation rate in aqueous ammonia via dissolution and reprecipitation mechanism [35]. The as-formed branched CuO nanoparticles induced higher electrochemical active surface area and thus more active sites, which facilitated CO_2 activation and the subsequent CO_2RR process. In addition, the accelerated CO_2RR process resulted in large consumption of protons in the solution and a rapid increase of the interfacial pH, which promoted the C–C coupling and the selectivity to ethylene. Thus, the design of Cu_2O with the branched CuO nanoparticles delivered a high FE of 70% for C_2H_4 at -1.05 V vs. RHE, which is superior to the original cubic Cu_2O NPs (FE = 32% at -1.05 V vs. RHE). Additionally, a 0D-Cu catalyst with dense vertical flake nanostructure (denoted as DVL-Cu) prepared by galvanostatic anodization induced a heterogeneous interface in the CO_2RR process, which not only effectively avoided agglomeration, but also reduced the C–C dimerization barrier in the C_2H_4 formation pathway, boosting the C_2H_4 selectivity (Fig. 6d-f) [122]. The Cu catalysts with sharp needle-like morphologies can also promote the C–C coupling and ethylene production due to their capability to nucleate and release small bubbles, leading to an increase in current density and mass transfer [123]. Cu nanoneedles were restored from $Cu_2(OH)_3Cl$ through the electroredeposition method. The total FE_{CO2RR} of this catalyst can reach 75% in 0.1 M $KHCO_3$ at -1.2 V vs. RHE and a high
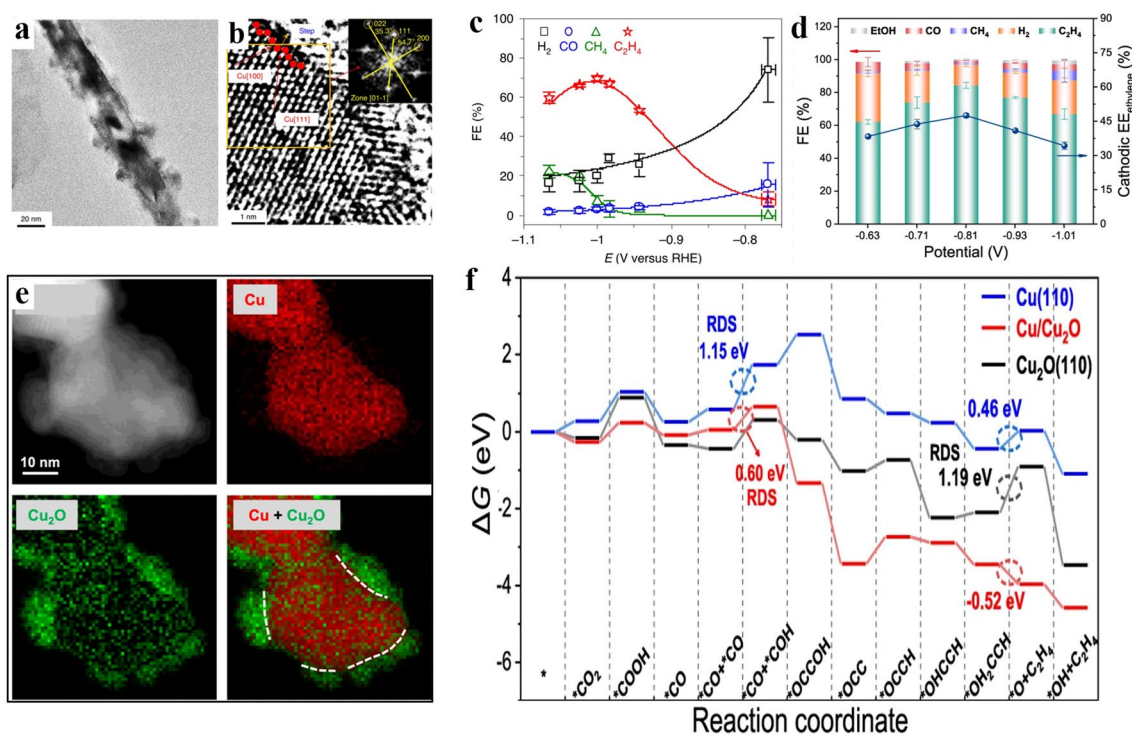

Fig. 6 a TEM image of A-CuNW. b HRTEM image of an A-CuNW with the step structure [27]. Reused with approval; Copyright 2020 Springer Nature. c FEs of A-CuNWs at -0.75 V to -1.1 V vs. RHE [121]. Reused with approval; Copyright 2018 Elsevier. d FEs and the selectivity of C_2H_4 of the DVL-Cu@GDL catalyst at -0.63 V to -1.01 V vs. RHE in the flow cell. e HAADF image and EELS maps in DVL-Cu. f Free energy diagram of the CO_2 to C_2H_4 on the Cu_2O(110) facet, Cu(110) facet and Cu/Cu_2O interface [122]. Reused with approval; Copyright 2022 Springer Nature

C_2H_4/CH_4 ratio of 200, demonstrating the preference for ethylene products over C_1 products.

4.1.2 Facets Effect

Altering the crystal facets can optimize the catalytic activity and selectivity of the catalysts due to the varied adsorption energy of intermediates on different crystal facets [124–126]. The early research results demonstrated that each facet of Cu may contribute to different product generations. For instance, Cu(100) was beneficial to the formation of C_2H_4, Cu(111) was easier to produce C_1 products, and Cu(110) prefer to C_2H_5OH and CH_3COO^- [127–129]. Therefore, reasonable adjustment of the exposed crystal facets can effectively regulate the corresponding catalytic performance of Cu-based catalysts.

It has been demonstrated that *CO intermediates are prone to be generated on Cu(100) facet compared to other Cu crystal such as Cu(110) and Cu(111), which tends to generate C_2H_4. Similarly, *CHO intermediates can also be easily formed on Cu(100), and two *CHO are dimerized to form C_2H_4. On the other hand, Cu(111) is more favourable for the formation of *COH intermediates, which generate both CH_4 and $HCOO^-$ [130, 131]. For example, three shaped Cu nanocrystals (NCs) with various facets have been prepared by a colloid method, and the one with Cu(100) delivered high productivity (FE = 57% at − 0.75 V vs. RHE) for C_2H_4 [132]. Nanocrystalline Cu with Cu(111) facet, however, has only 12% ethylene selectivity. Thus, increasing the proportion of Cu(100) facet on Cu-based catalysts is an efficient strategy to enhance the selectivity of C_2H_4. One example is the Cu foil with a controlled oxidation state and surface morphology derived by using CuCl as a precursor [26]. The stable surface of electropolished Cu(111) is converted to Cu(100) by using HCl to transfer the surface Cu(0) to Cu(I), followed by electrochemical reduction to achieve the reconstruction of Cu surface, leading to high FE for ethylene of 56% at − 2.0 V vs. Ag/AgCl. Moreover, selectively coating Cu(111) to achieve a higher (100)/(111) exposed facet ratio can also enhance the C_2H_4 production (Fig. 7b). Ultrathin Al_2O_3 has been utilized to be coated on Cu NCs by atomic layer deposition (ALD) technique resulted in a higher $FE(C_2H_4/CH_4)$ ratio of 22 times over pure Cu NCs (Fig. 7a) [133]. The coated catalyst reaches peak performance with a C_2H_4 FE of 60.4% at − 1.1 V vs. RHE and 300 mA cm^{-2} in 5 M KOH electrolyte in a gas diffusion electrode (GDE) flow cell (Fig. 7c). The results demonstrated that the presence of Cu(100) facet is critical for the selectivity to C_2H_4 in the CO_2RR process (Fig. 7d) [134]. The issue is that while Cu(100) is more conducive to the formation of C_2H_4, Cu(111) is the most stable facet of polycrystalline copper. Therefore, how to expose more Cu(100) and stabilize it in the CO_2RR process is important and challenging. It is shown that the surface energy of Cu(100) decreases significantly with the increase of the coverage of adsorbed species (including *CO, *COCHO, *COOH etc.) during CO_2RR, while the surface energy of Cu(100) changes slightly with the increase of the coverage of *H species during HER. The reaction intermediates adsorbed on the surface of Cu acted as capping agents which could benefit the growth of Cu(100). On the contrary, the adsorbed species did not affect the surface energy of Cu(111) either for HER or CO_2RR. Therefore, due to the lower surface energy of the formed adsorbed species on the Cu(100) facet, it is beneficial to reconstruct the polycrystalline Cu surface into Cu(100) in CO_2RR condition, while Cu(111) is more easily formed in HER condition [135].

The high-index facet, adding (111) or (110) steps to the (100) surface forming (Cu(711)(7(100) × (111)), can also boost the FE of ethylene [128]. For instance, the star-shaped Cu_2O nanoparticles with (322)(2(111) × (110)) facets prepared by the reductant-controlled method showed a high FE_{C2H4} value of 74.1% (at − 1.2 V vs. RHE) (Fig. 7e) [136]. DFT calculation revealed that the existence of Cu_2O(332) surface could significantly reduce the Gibbs free energy of the intermediate process (forming *CHO + *COOH, *CHO + *CO and *CHO + *CHO), thereby significantly improving the selectivity of C_2H_4 (Fig. 7f) [39, 137].

In addition to the crystal facet affecting, some non-traditional crystal phases can also effectively regulate the CO_2RR process. For instance, 4H Au@Cu and heterogeneous 4H/fcc Au@Cu core-shell nanostructures have been prepared by the epitaxial method with the wet chemical method (Fig. 7g) [28]. Both 4H Au@Cu and 4H/fcc Au@Cu delivered high partial current density (j_{C2H4}) and lower overpotential compared to the conventional face-centered cubic (fcc) Cu, which attributed to the low energy barrier of *CHO intermediates than *COH intermediates on the surface of 4H Cu, inducing preferable pathway for the formation of ethylene.
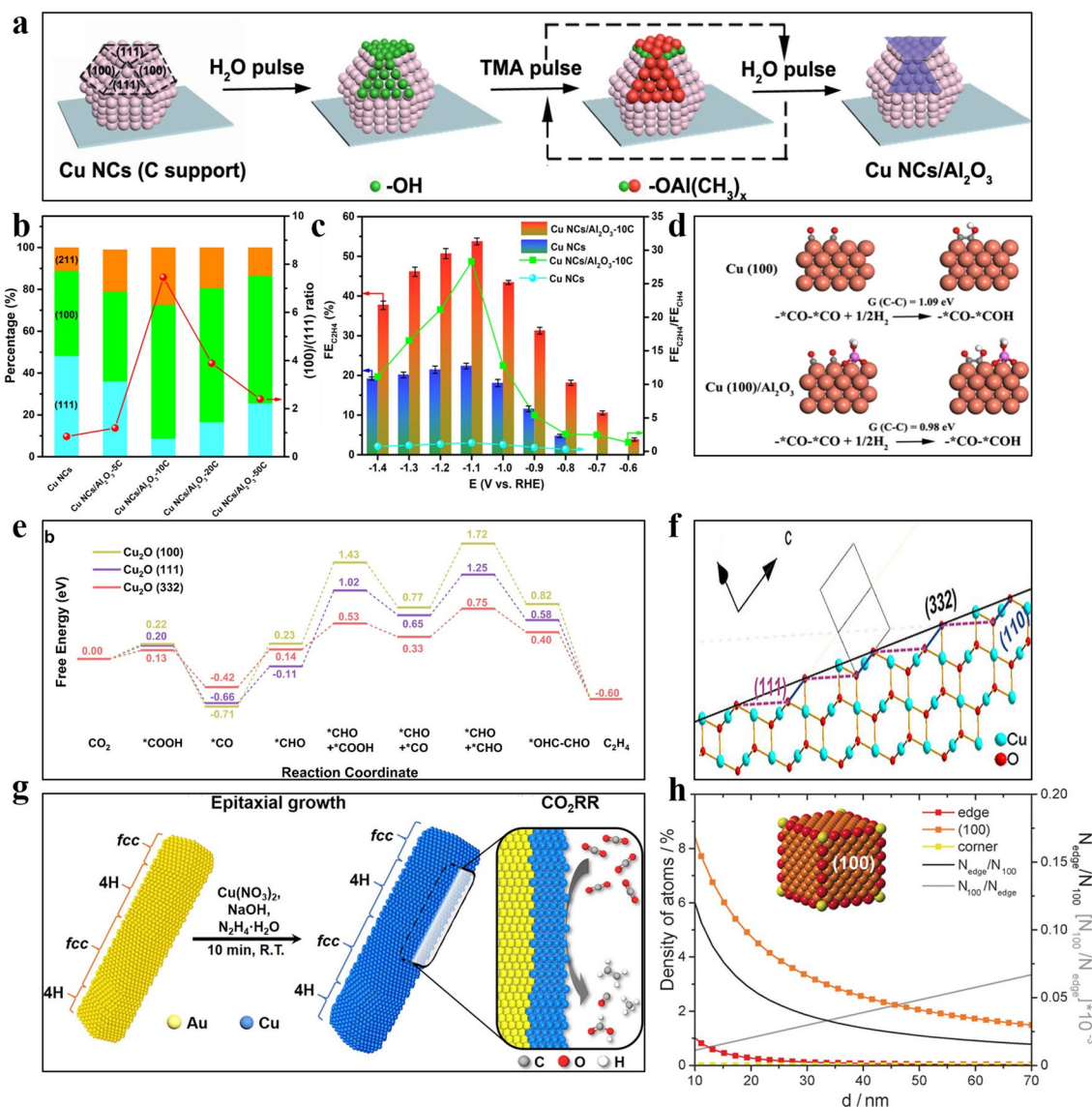
Fig. 7 **a** Schematic diagram of preparing FS-ALD with Al_2O_3 selectively coated Cu(111) facet. **b** (100)/(111) facet ratio and percentage of Cu nanocrystals with different Al_2O_3 coated cycles. **c** FE_{C2H4}/FE_{CH4} ratio and FE_{C2H4} of Cu NCs and Cu NCs/Al_2O_3-10C at -0.6 V to -1.4 V vs. RHE [133]. Reused with approval; Copyright 2021 Wiley. **d** Free energy of dimerized *CO and hydrogenation on Cu(100)/Al_2O_3 and Cu(100) [134]. Reused with approval; Copyright 2015 Royal Society of Chemistry. **e** Schematic diagram of the Cu_2O(332) facet. **f** Gibbs free energy of the reaction intermediates on Cu_2O(100) (111) and (332) facet [136]. Reused with approval; Copyright 2022 Wiley. **g** Schematic diagram of synthetic 4H/fcc Au@Cu nanorods [28]. Reused with approval; Copyright 2020 American Chemical Society. **h** Relationship between the edge length **d** and the density of the adsorption site and the N_{edge}/N_{100} in Cu NC cubes [139]. Reused with approval; Copyright 2014 American Chemical Society

4.1.3 Size Effect

The size of electrocatalysts directly changes the coordination environment of the surface atoms and thereby influences the CO_2RR catalytic activity and selectivity. Decreasing particle sizes increases surface curvature and lowers the average coordination number of surface atoms [5, 138]. The small size of the Cu catalysts (< 15 nm) may result in the strong adsorption activity of *CO on the low coordinated Cu atoms, leading to the production of H_2 and CO. With the increase of the size, the proportion of edge sites and corners sites decreases, and thus the generation of H_2 and CO is suppressed [139]. However, the large size of catalysts

may reduce edge active sites, resulting in unsatisfactory catalytic activity (Fig. 7h). Therefore, optimizing the size of Cu catalysts for CO_2RR is highly favourable to generate desired products. For instance, three Cu cubes with a size of 24, 44 and 63 nm, were prepared by adjusting the reflux temperature and aging time. The Cu cubes with 44 nm have exhibited a maximum FE_{C2H4} of 41% (at -1.1 V vs. RHE) in 0.1 M $KHCO_3$ originating from the ideal ratio of plane sites on Cu(100) to edge sites [140]. The size effect can also influence the unsaturated edge sites, which is also significant to the CO_2RR selectivity, resulting in optimized binding strength of the reaction intermediates [100]. For example, Cu nanoparticles with varied sizes were derived by electro-reducing the pre-prepared Cu_2O film [141]. The experimental results showed that FE_{C2H4} was inversely proportional to the size of the catalysts, in which the size decreased from 41 to 18 nm, while the FE of C_2H_4 increased from 10% to 43%. The smaller Cu particles with higher selectivity for C_2H_4 were attributed to more grain boundaries and defects, which significantly enhanced the *CO adsorption and thus the C–C coupling step. Although the above two examples showed contradictory conclusions regarding the size of the Cu nanoparticles, the induced effect by altering the catalyst's size such as increasing crystal facet (former), active sites (latter), and stronger *CO adsorption energy (latter) is more important for promoting ethylene production.

4.2 Molecular Catalysis

Molecules can change the coordination environment of Cu atoms in the catalysts, and the interaction between catalysts and ligands can stabilize the key intermediates. It has been widely studied that modifying Cu by organic macro-molecules can form complexes that may be beneficial for ethylene production [142, 143]. For instance, Cu porphyrin (PorCu) and Cu phthalocyanine (CuPc) composed of Cu^+ and macrocyclic complexes have been investigated to selectively reduce CO_2 to ethylene [144]. PorCu and CuPC have a tuneable molecular structure and a larger conjugated system, which makes it easier to adjust the electronic structure of center Cu^+. Moreover, ProCu has exhibited high selectivity and activity to C_2H_4, attributing to the OH group in the porphyrin structure as binding sites to the reaction intermediates. It can also provide intramolecular sources of

protons, with an oxidation state of Cu^+ at the center as the active sites [145]. Another example is the surface of the Cu cluster engineered by controlling the paddle-wheel structure of the Cu dimer in the deformed HKUST-1 ($C_{18}H_6Cu_3O_{12}$, $Cu_3(BTC)_2 \cdot xH_2O$, BTC = benzene-1,3,5-tricarboxylate) MOF [33]. It was found that the Cu clusters with the asymmetric structure were formed from the deformed Cu dimers by heat treatment, resulting in more uncoordinated Cu sites, which were able to increase the FE of C_2H_4 from 10% to 45% while reducing the H_2 yield to less than 7%. Recently, a local sulphur doping strategy has been used to rationally construct isolated Cu-S (S-HKUST-1) on HKUST-1 pre-catalyst (Fig. 8a) [146]. The catalyst was reconfigured in situ to obtain a two-phase copper/copper sulphide (Cu/Cu_xS_y) interface with abundant $Cu^{\delta+}$ sites (Fig. 8b). The moderate coupling site distance of stable $Cu^{\delta+}$ reduced the kinetic barrier for the dimerization of the *CO intermediates, demonstrating a high C_2H_4 selectivity up to 57.2% at -1.32 V vs. RHE at the operated a j of 400 mA cm^{-2} (Fig. 8c, d). Moreover, dual active sites with PcCu-$(OH)_8$ as ligands and square planar CuO_4 as nodes (PcCu-Cu-O) have been investigated for highly efficient CO_2RR [147]. The results demonstrated that the derived PcCu-Cu-O exhibited up to 50% FE_{C2H4} and a high current density of 7.3 mA cm^{-2} at -1.2 V vs. RHE. The excellent catalytic activity and selectivity are attributed to the synergistic effect between PcCu (*CHO formation sites) and CuO_4 (*CO formation sites), reducing the energy barrier of C–C coupling step (easier than the direct coupling of *CO intermediates), thus boosting the ethylene selectivity in CO_2RR process (Fig. 8e). Another flexible and tunable Cu(I) triazole framework was also developed as a novel MOFs material for electrocatalytic CO_2 reduction, in which the Cu_2O and dialkyl-1,2,4-triazoles were reacted to produce isoreticular analogs of MAF-2 ([Cu(detz)], Hdetz = 3,5-diethyl-1,2,4-triazole) [148]. By changing the size of the non-coordinating ligand side groups, MAF-2E (i.e., MAF-2, side group are two ethyl groups) was derived, resulting in high FE_{C2H4} up to 51.2% (-1.30 V vs. RHE) and excellent stability over 10 h. Computational simulations showed that compared with MAF-2P (side group are two propyl groups), although the binuclear copper sites in the structure could allow the intermediate to have C–C coupling, the smaller ethyl groups had less spatial steric resistance to binuclear Cu sites, which are more favourable for the C–C coupling process to promote the C_2H_4 generation (Fig. 8f–i). Moreover, the side groups of two ethyl groups increased the
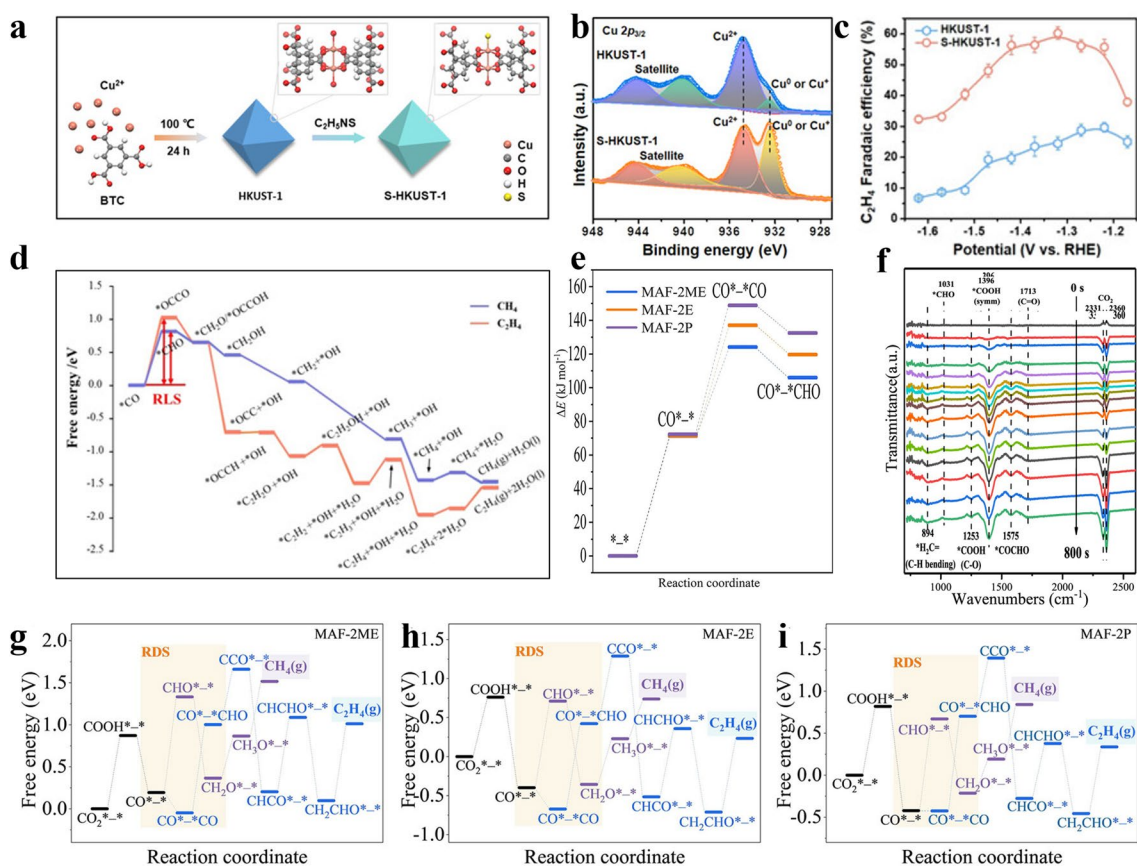
Fig. 8 **a** Schematic diagram of preparation of S-HKUST-1 doped with S atom. **b** XPS spectra of S-HKUST-1 catalysts in the Cu_{2p} region. **c** FE_{C2H4} of HKUST-1 and S-HKUST-1 at −1.15 to −1.6 V vs. RHE. **d** Free energy illustrations for obtaining C_2H_4 and CH_4 on Cu(111) facet [146]. Reused with approval; Copyright 2022 Wiley. **e** In-situ ATR-FTIR spectra of PcCu-Cu-O during the process of electroreduction of CO_2 to ethylene [147]. Reused with approval; Copyright 2021 American Chemical Society. **f** Framework energies of the catalysts at different CO_2RR states. The free energy graphic of **g** MAF-2ME, **h** MAF-2E and **i** MAF-2P in proper order [148]. Reused with approval; Copyright 2022 Wiley

hydrophobicity of the material and inhibited the competition of HER.

4.3 Alloy Effect

By combining two or more complementary metals into heterogeneous catalysts, the selectivity, activity and stability of these catalysts can be further improved for CO_2RR due to the altered electronic structure and geometric effects [5, 45, 60]. Recently, alloying different metal species with Cu to form bimetallic catalysts has been widely investigated, which showed a significant change in selectivity. For instance, CuIn and CuAu are reported to improve the FE of CO, while CuSn and CuPd can promote the

production of $HCOO^-$ [60]. CuAg and CuZn, on the other hand, are slightly different. The main products for CO_2RR using these two catalyst species can be easily altered by changing the metal ratios and preparation methods.

It has been established that the concentration of *CO on catalysts is a decisive factor in determining the selectivity of CO_2RR to ethylene. Forming alloys by introducing foreign metals (e.g., Ag, Zn, Au, Zr) to Cu can convert CO_2 to *CO more efficiently, which increases the local *CO concentration around the Cu sites [10, 41, 149–155]. It has been confirmed by operando Roman Spectroscopy that in AgCu alloys, the *CO intermediates initially formed on Ag sites, which were then transferred to the Cu sites for spillover and hydrogenation (Fig. 9b–e) [156]. To confirm this, the nanoporous CuAg catalysts with varied Ag content (3%–9%)
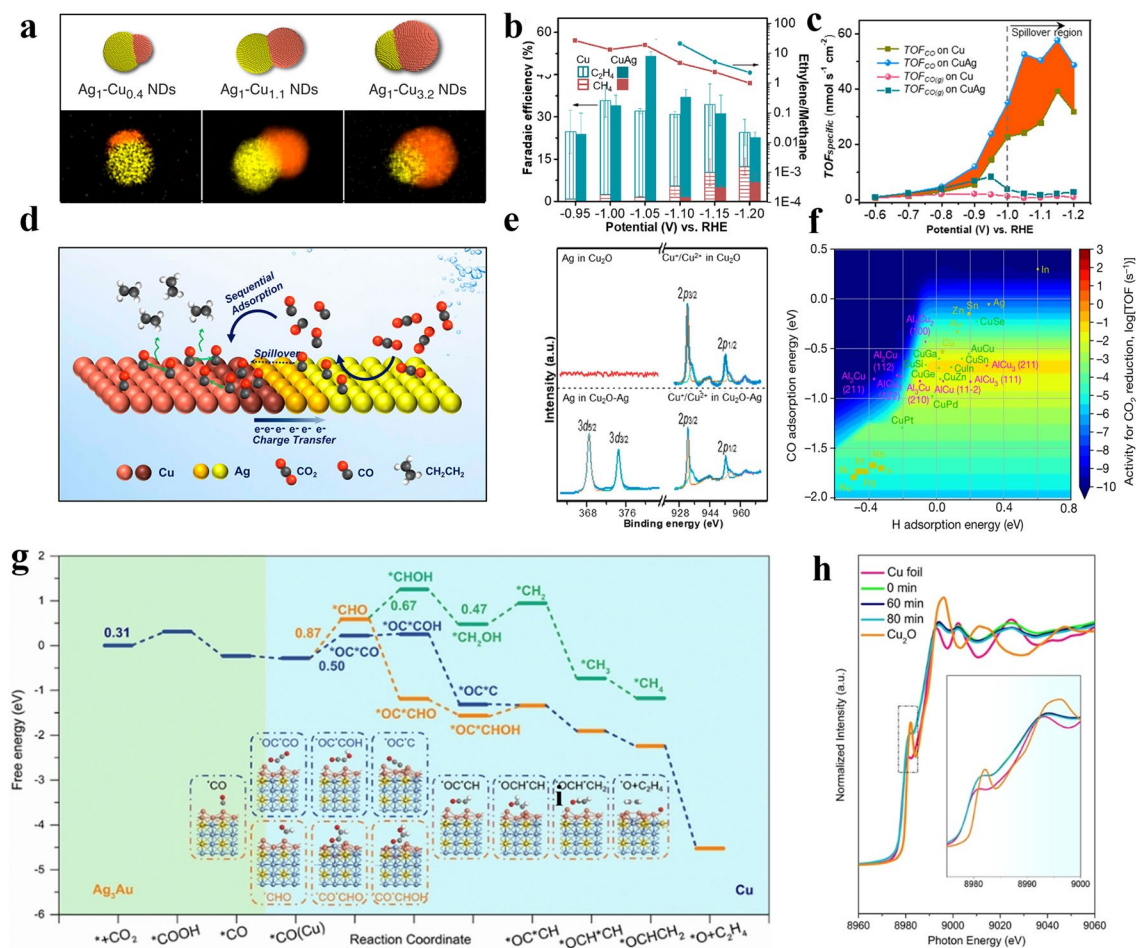
Fig. 9 **a** Schematic and EDX elemental mapping of Ag (yellow) and Cu (orange) of $Ag_1-Cu_{0.4}$ nanodimers, $Ag_1-Cu_{1.1}$ nanodimers and $Ag_1-Cu_{3.2}$ nanodimers [159]. Reused with approval; Copyright 2019 American Chemical Society. **b** FE_{C2H4} FE_{CH4} and FE_{C2H4}/FE_{CH4} on Cu and CuAg catalysts. **c** The formation rate of CO at the Ag site in CuAg. The orange part indicated that the addition of Ag promotes the formation of CO. **d** Schematic diagram of the proposed mechanism of CO_2 conversion C_2H_4 in the AgCu tandem catalyst. **e** XPS spectra of Cu $2p$ and Ag $3d$ of Cu_2O-Ag and Cu_2O [156]. Reused with approval; Copyright 2022 Wiley. **f** 2D activity volcano plot for CO_2 reduction [30]. Reused with approval; Copyright 2020 Springer Nature. **g** Free energy of intermediates with the reaction coordinates following the route towards CH_4 and C_2H_4. **h** Operando Cu K-edge XAFS spectra of Cu_3-Ag_3Au nanoframes at a different time [163]. Reused with approval; Copyright 2021 Wiley

have been achieved by the electrodeposition method, and the results indicated that the Ag content influenced the selectivity of CuAg alloys [154]. The low Ag content of 3% decreased the chance to form C_2H_4, and the high Ag content of 9% led to the generation of CO by inducing the separated atomic structure [157, 158]. CuAg alloys with appropriate Ag value (6%) resulted in the highest yield of C_2H_4 (FE = 60% at − 0.7 V vs. RHE and a total current density of − 300 mA cm^{-2}). The regulated CO_2RR performance by changing the Ag content is attributed to the alteration of the concentration of surface *CO intermediates, which is more conducive to the C–C coupling on Cu sites, which boosted ethylene production. Another example is the AgCu alloy with

heterojunction structure which showed the highest yield of C_2H_4 with FE = 42% (at − 1.10 V vs. RHE) with Ag content of 6 wt% (Fig. 9a) [159]. The continuous increase of Ag content led to the aggregation of nanoparticles and decrease the catalytic activity. Moreover, the electronic effect induced by the Ag/Cu dual metal alloy catalysts is another factor affecting product selectivity [160]. The results showed that the emergence of the Ag/Cu interface caused electrons to move from the Cu domain to the Ag domain [160]. The electron-depleted Cu could efficiently enhance the binding of *CO on the active sites, which in turn facilitates the coupling of *CO into C_2H_4. Owing to the *CO spillover effect and electron

transfer effect of tandem catalysis, the selectivity of C_2H_4 was further improved in CO_2RR.

Zn atoms play a similar role to the above-mentioned Ag when alloying with Cu to selectively promote ethylene production. For instance, the mixed CuZn NPs with homogeneous elemental distribution have been derived from the ablation of CuZnO alloy using a nanosecond pulse laser [161]. The uniform distribution of Cu and Zn atoms efficiently reduced the transfer distance of the formed *CO intermediates from Zn sites to the nearby Cu sites, thus reducing the reaction barrier and facilitating the C_2H_4 generation. Similarly, incorporating active metal Al into Cu forming Cu-Al alloy can also enhance C_2H_4 production (Fig. 9f) [30]. The as-prepared Cu-Al alloy possessed the highest number of *CO adsorption sites, and the *CO adsorption energy (ΔE_{CO}) produces near-optimal activity. The water near the Al atoms efficiently reduced the generated *HOCCH to *CCH, which could not only decrease the formation energy, but also inhibits the production of competing alcohols, leading to the selectivity of C_2H_4 (FE = 80% at −1.5 V vs. RHE and at a current density of 400 mA cm^{-2}). Different from Zn and Ag to promote the formation of *CO intermediates, Pd possesses stronger adsorption of proton, which can also promote the generation of C_2H_4. For instance, phase-separated CuPd alloy with adjacent Cu atoms (phase separation) was beneficial to the production of C_2H_4, whereas the one with alternating Cu-Pd arrangement preferred the production of CH_4 [162]. The adjacent characteristics of Cu atoms allowed favourable molecular distance and small spatial steric hindrance, making the adjacent adsorbed *CO easily dimerize into *COCOH intermediates with the aid of Pd, which were then converted into C_2H_4 (FE = 48% at −0.7 V vs. RHE and the highest total current density of 370 mA cm^{-2}). In addition, the ternary Cu-Au/Ag nanoframes could also efficiently promote the reduction of CO_2 to C_2H_4 [163]. Alloyed Ag/Au nanoframes have been recognized as one of the most efficient CO-specific catalysts, and the design of nanopore frameworks is also conducive to the exposure of active centers while promoting mass transfer. The derived Cu-Au/Ag nanoframes have exhibited a maximum value of $FE_{C2H4} \approx 79\%$ at −0.65 V vs. RHE in the flow cells (Fig. 9g, h). The improved C_2H_4 production was ascribed to the integrated tandem catalysis (*CO was formed on the Ag/Au nanoframes and then spill over to Cu for coupling), electronic modulation (Cu conducts electrons to Ag/Au) and defect engineering (Ag/Au framework with many defects).

4.4 Defect Effect

The defects can also play a significant role in the electrocatalysis process, such as optimizing the reaction barrier, increasing the number of active sites, and inhibiting the competitive reaction HER, thus promoting catalytic activity and selectivity [100, 110, 164, 165].

4.4.1 Metal Defects

Metal defects optimize the CO_2 conversion to C_2H_4 by altering unsaturated coordination atoms, electronic band structure and local charge distribution. For example, the prism-shaped Cu catalysts with metal defects increased C_2H_4 yield due to the possible change of local pH and the formation of low-coordinated Cu atoms on the rough prism surface [166]. Cu nanosheets with 6 nm defects size also enhanced the FE_{C2H4} to 83% at −1.2 V vs. RHE [25]. The high performance was ascribed to the induced defects, which are beneficial to the adsorption, enrichment and restriction of reaction intermediates (*CO and *OCCO) and OH$^-$, thus promoting the C–C coupling for ethylene production. The effect of pore defects on the performance of C_2H_4 generation has also been studied. Changing the pore size and depth can significantly influence the selectivity of designed catalysts. When the pore width was reduced to 30 nm, the formation of C_2H_4 increased from 8% to 38%, while the C_1 gas products decreased (FE_{CO} = 5% and FE_{CH4} = 15%) [167]. The enhanced C_2H_4 selectivity is attributed to the restriction of proton transmission and the increased local pH, which is conducive to the occurrence of C–C coupling. Moreover, grain boundaries have been investigated as a kind of defect by designing a unique planetary-like Cu structure via structural reconstruction (Fig. 10a, b) [168]. A large number of Cu grain boundaries were produced during the reconstruction process due to the fusion of components in the ultrafine Cu particles. The components in the shell were separated to form a nano-gap structure, which could effectively limit OH$^-$ on the surface of catalysts to maintain a high local pH value, thus promoting C_2H_4 production (Fig. 10c–f).

4.4.2 Vacancies Defects

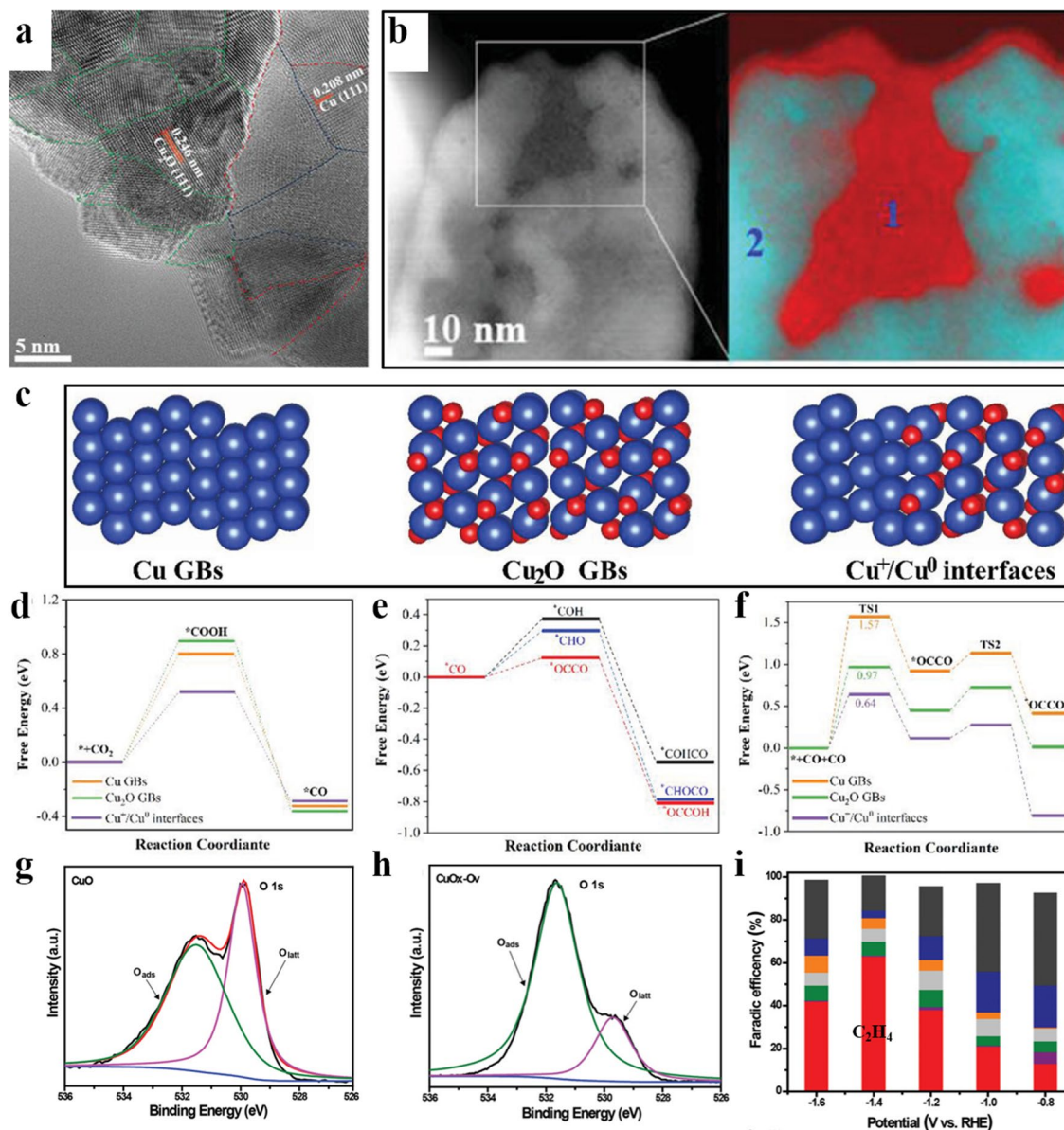In addition to metal defects, oxygen vacancies have also been investigated to selectively boost C_2H_4 production.

Fig. 10 a HRTEM image with magnified region of GBs. **b** EELS mapping of Cu^+ in 1 and Cu^0 in 2. **c** DFT calculations models for Cu GBs, Cu_2O GBs, and Cu^+/Cu^0 interfaces. The free energy on Cu GBs, Cu_2O GBs, and Cu^+/Cu^0 interfaces of **d** CO_2 to produce *CO, **e** *CO formate different C_2 intermediates, **f** *CO dimerization to obtain *OCCO and subsequent *OCCO conversion to *OCCOH [168]. Reused with approval; Copyright 2022 Wiley. XPS spectra of O 1s of **g** CuO and **h** CuO_x-Vo. **i** FE_{C2H4} of CuO_x-Vo [169]. Reused with approval; Copyright 2019 Wiley

These oxygen vacancies can not only generate unsaturated metal ions, but also induce the charged positions as trap sites for electrons or holes [45]. For instance, highly branched CuO_x nanodendrites with a high surface density of Vo's (referred to as CuO_x-Vo) prepared by a two-step thermal annealing and electrochemical reduction technique showed a high FE_{C2H4} of about 63% at -1.4 V vs. RHE (Fig. 10g, h) [169]. This Vo's possessed weakly bound electrons, which

make them excellent Lewis base sites to adsorb CO_2 and transfer electrons to the intermediate of $CO_2{}^{\cdot-}$. Therefore, Vo's is functional to optimize the adsorption energy of reactants and promote molecular activation, leading to the strong adsorption energy of *CO/*COH intermediates and rapid desorption of *CH_2 (2*$CH_2 \rightarrow C_2H_4$).

In addition to O vacancies, other anionic defects such as S and N vacancies have also been found to have an impact

on CO_2 reduction products. Due to the high mobility of S atoms in complex CuS crystal structures, it is easy to produce stable surface defects [170, 171]. For example, a copper sulfide-copper core-shell catalyst rich in surface vacancies (Cu_2S-Cu) was synthesized by using enriching vacancy Cu_2S nanoparticles as precursors, which can achieve high selectivity for C_2H_4 (45% at -1.1 V vs. RHE) [172]. The introduced vacancies on the Cu shell can efficiently modify the electronic structure of adjacent Cu atoms, which can affect the energy barrier of the rate-limiting reaction intermediates. It is worth noting that when the proportion of vacancies on the surface increases, the energy barrier for ethylene formation will be slightly increased, but ethanol will not be affected, so the selectivity of the product will be transferred from C_2H_4 to multi-carbon alcohols. Therefore, optimized vacancy degree can contribute to the ethylene production [173]. Recent studies have also shown that N vacancies possess higher stability than O vacancies due to the high metal-N bond energy in transition metal nitrides [174, 175]. Cu_3N_x with different nitrogen densities were prepared by a lithiation-enabled vacancy-engineering strategy, and the nitrogen vacancy densities highly affect the adsorption energy of *CO and the energy barrier for the formation of key C_2 intermediates [176]. These presented N vacancies led to a decreased distance between adjacent Cu atoms, which is beneficial to the bonding of *CO absorbed at Cu sites [177]. The FE of Cu_3N_x with 50% of N vacancy concentrations for C_2 products is 81.7% ($FE_{C2H4} = 56\%$) at -1.15 V vs. RHE [176]. The Cu_3N_x catalyst also showed excellent electrochemical stability at high current density ($j = -350$ mA cm^{-2}, 10,000 s, FE_{C2} dropped from 82.1% to 76%), which greatly surpasses the CuO_x catalyst with oxygen vacancies ($j = -350$ mA cm^{-2}, 850 s, FE_{C2} dropped from 63% to 43%).

4.4.3 Non-metal Doping

Incorporating non-metal is another technique to introduce defects in Cu-based catalysts. For instance, Cu_3N nanocube with perovskite structure preferred the coupling of *CO and *CHO thus enhancing the C_2H_4 production [178]. $Cu_{1.8}Se$ nanowires grown on 3D copper foam substrates also exhibited excellent capability to produce ethylene, reaching the maximum value of FE_{C2H4} of 55% at -1.1 V vs. RHE [179]. The results showed that the introduction of Se can reduce the surface concentration of *CO and inhibit the formation of C_1

products. In addition, fluorine-modified copper (F–Cu) introduced a new view on the mechanism of "hydrogen-assisted C–C coupling" [39]. Fluorine modification not only is conducive to the activation of H_2O to form active hydrogen species (*H), but also promotes the adsorption and hydrogenation of *CO to produce *CHO intermediates, which can be easily coupled and reduced to C_{2+} products on the Cu surface. Other than single non-metal elements, silicon dioxide has also been introduced into Cu by one-pot coprecipitation method to create active Cu-SiO$_x$ interface sites, which reduced the formation energy of key intermediates OCOH* and OCCOH* during ethylene production [180].

4.5 Surface Modification

Changing the hydrophobicity at the interface between catalysts and electrolyte, such as incorporating molecules to modify the surface of catalysts, is an efficient approach to inhibit HER, facilitate the mass transfer of CO_2, and optimize the adsorption/desorption of intermediates, thus boosting the catalytic activity and selectivity of CO_2RR to ethylene. Moreover, increasing pH at the hydrophobic interface is also conducive to the occurrence of C–C coupling [181]. For instance, coating different hydrophilic/hydrophobic polymers on CuO nanoparticle (NPs) electrodes can efficiently alter the electrode-electrolyte interface in CO_2RR process (Fig. 11a, b) [182]. It was demonstrated that hydrophilic polymers played negligible roles in altering the catalytic performance, whereas hydrophobic polymers can significantly improve the activity, selectivity and stability of CuO derivative electrodes to boost C_2H_4 generation (Fig. 11d). The experimental results demonstrated that the enhanced performance was mainly attributed to the constructed hydrophobic microenvironment of the gas/liquid/solid three-phase interface on the electrode surface, which limited the water diffusion, improved the local pH near the electrode surface, and then improved the performance of CO_2RR process (Fig. 11c, e) [32, 183, 184]. The incorporated polymers can also work as the protective layer of the catalysts. For example, introducing N'N-ethylene-phenanthrolinium dibromide in Cu catalysts can efficiently etch the surface to form cubic nanostructures and stabilize the nanostructures in the electrocatalysis process by forming a protective organic layer, resulting in a high selectivity of 45% for C_2H_4 at -1.07V vs. RHE [185]. Moreover, a molecular regulation strategy
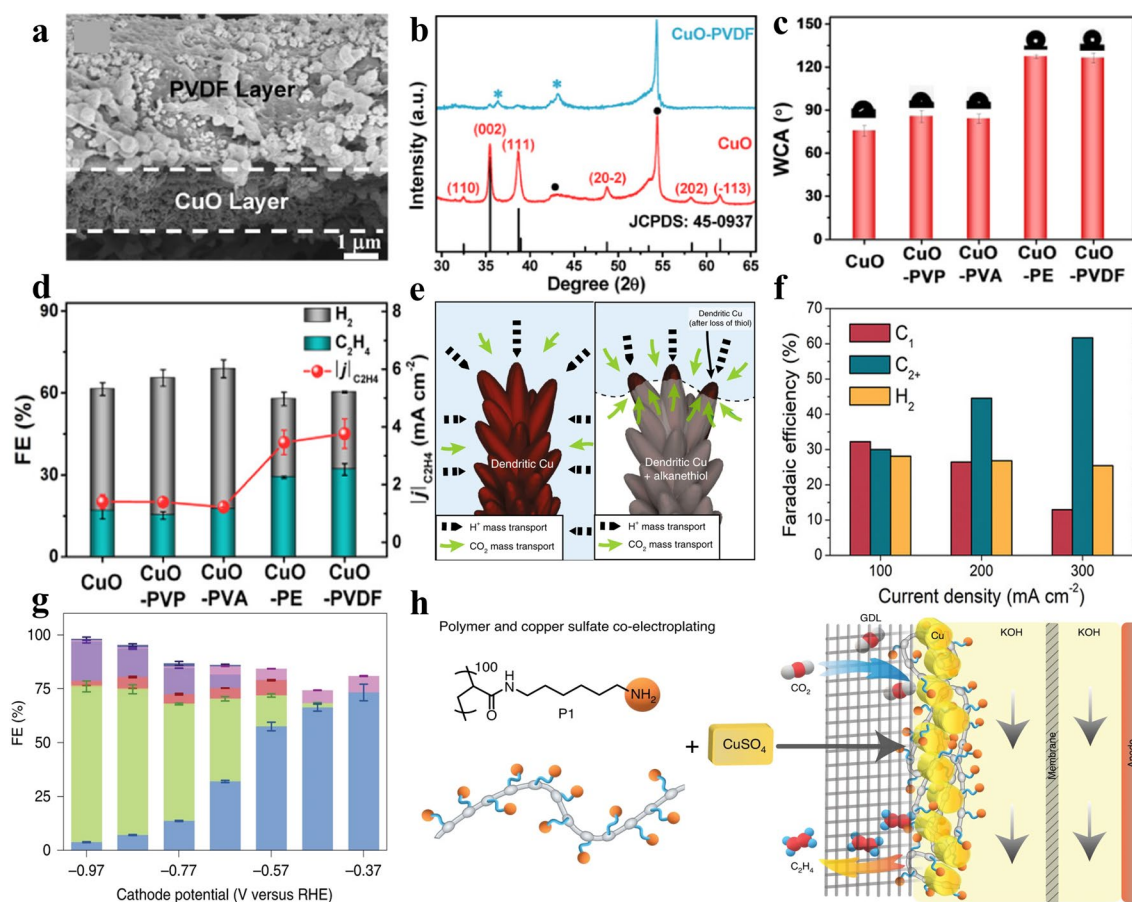
Fig. 11 a Cross-sectional morphology in SEM pictures. **b** XRD pattern compared with standard CuO-PVDF, where "*" denotes diffraction peaks from PVDF and "•" from graphite [182]. Reused with approval; Copyright 2021 American Chemical Society. **c** Water contact angles, **d** FE_{C2H4}, FE_{H2} and j_{C2H4} for CuO surface modified with PVP, PVA, PE, and PVDF [185]. Reused with approval; Copyright 2019 Wiley. **e** Mass transfer diagram of non-hydrophobic and hydrophobic dendrites [32]. Reused with approval; Copyright 2019 Springer Nature. **f** FE of C_1, C_{2+} products and H_2 at 3 kinds of current densities [34]. Reused with approval; Copyright 2019 Wiley. **g** FE of all products on Cu-P1 at the range of -0.37 V to -0.97V vs. RHE. **h** Schematic illustration of synthetic Cu-P1 on the GDL [186]. Reused with approval; Copyright 2021 Springer Nature

by functionalizing the electrocatalysts with organic molecules can stabilize the intermediates (*CO) and promote the conversion of CO_2RR to ethylene [14]. The incorporation of organic polymers with specific functional groups has been investigated to tune the selectivity of the CO_2RR process. The Cu-poly-N-(6-aminohexyl)acrylamide (denoted as Cu-P1) prepared by the coprecipitation method boosted the ethylene selectivity up to 72% at -0.97 V vs. RHE in 1 M KOH (Fig. 11g) [186]. A series of stable Cu electrodes modified by amine-containing additives with different methylation degrees were prepared by controlling the amount of methyl to replace the hydrogen atom on P1. The results demonstrated that the CO_2RR selectivity was dependent on

the degree of methylation of P1 on the Cu-P1 electrode, in which the ethylene yield decreased with the increase in the degree of methylation in the polymer, whereas the HER process was the opposite trend. Amino groups also play a key role in boosting the C_2H_4 generation by contributing to the CO_2 capture and leading to local pH increase on the electrode surface (Fig. 11h). Ionic liquids (IL) coated on the Cu catalysts are responsible for the improved conversion efficiency of CO_2 to ethylene, which is attributed to their strong CO_2 solubility, effectively increasing the CO_2 concentration in the reaction phase and improving the equilibrium conversion rate. On the other hand, the strong hydrogen bond and static electricity between ionic liquids and CO_2 show suitable

reaction energy, which can partially activate CO_2 double bond and achieve stronger adsorption of *CO intermediates [187, 188]. For instance, IL BmimNO$_3$ (IL 1-butyl-3-methylimidazolium nitrate) on Cu electrocatalyst delivered FE = 77.3% for ethylene selectivity at −1.49 V vs. RHE [189]. The high CO_2RR performance was ascribed to the activation of CO_2 molecules on IL, the changed coordination environment of Cu atoms, regulated local electronic structure, and the boosted *CO dimerization rate. Moreover, the hydrophobic carbon chain in BmiNO$_3$ increased the CO_2 concentration at the electrode-solution interface, thus inhibiting the competition of HER and improving the efficiency of CO_2RR.

4.6 Valence State

The valence state of metal atoms also plays an important role in the selectivity of CO_2RR [190]. When the surface Cu atoms are partially positively charged, the synergistic between $Cu^{\delta+}$ and Cu^0 causes strong electrostatic adsorption of the negatively charged *CO intermediates on the active sites, reducing the C–C coupling energy barrier and promoting ethylene formation [191]. For instance, Cu_2O with Cu^+ was covered by the reaction intermediates (such as *CO) on the surface in the CO_2RR process, which effectively prevents Cu^+ from being reduced to Cu [192]. Cu^+ has lower adsorption energy of *CO intermediate than Cu, so it can improve the coverage of *CO and promote C–C coupling. The achieved catalyst reached a maximum C_{2+} FE of 75.2% at a potential of −0.61 V vs. RHE. Moreover, the catalysts with a mixed valence state may exhibit superior performance compared to the ones with a single valence state [193]. In the Cu^0–Cu^+ system, the Cu^0 functioned to activate CO_2 and promote the subsequent electron transfer, meanwhile Cu^+ site enhanced the adsorption of *CO, thus further promoting C–C coupling [194–197]. The selectivity of the catalysts with Cu^+/Cu interface to C_2H_4 can reach 40% at −1.0 V vs. RHE, while very little C_2H_4 (less than 5%) has been observed on pristine Cu catalysts. In addition, Cu_4O_3 with the same amount of Cu^+ and Cu^{2+} ions were prepared by the solvothermal method, which acted as pre-catalysts to form the intrinsic active sites (Cu^0, Cu^+ and Cu^{2+}) after partial reduction [34]. The active sites with mixed valence states can not only reduce the energy barrier in forming C–C

bonds, but also possess the capability to electrostatically stabilize *OCCO intermediate. The FE_{C2H4} was 43% at −0.64 V vs. RHE, and the highest C_{2+}/C_1 product ratio of 4.8 has been achieved at the same condition (Fig. 11f). Table 1 summarizes the performance of CO_2 to ethylene for the Cu-based catalysts, including FE, current density, durability, electrochemical cell type, GDE structure, and electrolyte selection.

5 Conclusions and Perspectives

The rational design of Cu-based electrocatalysts for ethylene production with high energy density and selectivity is one of the most significant goals in CO_2RR. In this review, we have summarized the key steps to convert CO_2 to ethylene, including CO_2 adsorption/activation, formation of *CO intermediate, and the C–C coupling step. An in-depth understanding of these key steps provides an intrinsic mechanistic investigation of fundamental principles for the CO_2RR process. The microenvironment (pH effect, cation/anion effect), facet, *CO intermediates, overpotential and additives influence on CO_2RR to generate ethylene or other competitive products have been discussed to propose the preferred reaction pathways and conditions to selectively produce ethylene. The catalyst preparation and surface engineering at the atomic level can significantly affect the interface microenvironment, thus the selectivity from CO_2 to ethylene. The strategies of nanostructures control, molecular catalysis, alloy, defect engineering, surface modification, and oxidation state alteration to engineer the Cu-based catalysts have been summarized and discussed. The summarized recent progress of research work demonstrated that the engineered strategies are highly associated with the binding energies of intermediates (optimize the binding energy for specific intermediates), thus controlling the catalytic activity, selectivity and product distribution of CO_2RR.

Currently, tremendous progress has been achieved for CO_2RR based on experimental and computational methodologies, resulting in many breakthroughs for CO_2 converting to ethylene or other C_{2+} product. However, it is still challenging to specifically generate single specific products as it is difficult to control the engineering strategies to have no influence on other intermediates or products. Therefore, it is still necessary to address the fundamental issues related to CO_2RR to achieve continued development and practical application.

Table 1 A summary of recent advances in CO_2 electroreduction to C_2H_4

Strategy	Catalyst	Electrolyte	FE_{C2H4} (%)	E (V vs RHE)	j_{C2H4} (mA cm^{-2})	GDE structure	electrochemical cell	durability (h)	Refs.
Nanostructure effect	Cu-I	0.1 M KHCO$_3$	80	−0.9	31.2	–	H-cell	22	[198]
	OBC	0.5 M KHCO$_3$	45	−0.95	44.7	–	H-cell	10	[199]
	4H Au@Cu nanoribbon	0.1 M KHCO$_3$	44.9	−1.11	14.4	–	H-cell	–	[28]
	KB@Cu$_3$ (HITP)$_2$	0.1 M KHCO$_3$	70	−1.37	26.5	–	H-cell	10	[200]
	Cu-mesocrystal	0.1 M KHCO$_3$	27.2	−0.99	6.8	–	H-cell	6	[134]
	CuAl-1	0.1 M KHCO$_3$	82.40	−0.99	–		H-cell	100	[201]
	Cu-N-C-800	0.1 M KHCO$_3$	24.8	−1.4	6.84	–	H-cell	10	[202]
	DVL-Cu	0.5 M KCl	84.5	−0.8	92.5	–	MEA	55	[122]
Molecular catalysis	Cu-12	1 M KHCO$_3$	72	−0.83	232	PTFE	Flow-cell	190	[14]
	PcCu-Cu-O	0.1 M KHCO$_3$	50	−1.2	7.3	–	H-cell	4	[147]
	Ag@BIF-104NSs (Cu)	0.5 M KHCO$_3$ + 0.5 M KCl	21.43	−1.2	4.36	–	H-cell	4	[203]
	S-HKUST-1	1 M KHCO$_3$	60.0	−1.30	20	–	H-cell	8	[146]
	CTPI	0.1 M KHCO$_3$	66	−3.7	208	PTFE	Flow-cell	100	[204]
	A-CuNW	0.1 M KHCO$_3$	77.4	−1.01	22.4	–	H-cell	200	[27]
	IL@Cu	0.1 M KHCO$_3$	77.3	−1.49	34.2	–	H-cell	3	[189]
	C/HKUST-1/ Cu/PTFE	1 M KOH	49.1	–	491	PTFE	Flow-cell	65	[37]
	Cu-PzH	1 M KOH	60	−1.0	346	CP	Flow cell	3.9	[205]
	GMC- [Cu$_2$(NTB)$_2$]	0.1 M KCl	42	−1.28	–		H-cell	2	[206]
	AuNN@PCN-222(Cu)	0.1 M KHCO$_3$	52.5	−1.2	–	–	H-cell	10	[207]
Alloy effect	Cu-Al	1 M KOH	80	−1.5	400	PTFE	Flow-cell	50	[30]
	Cu/NiNC	1 M KOH	40	3.2	150	–	MEA	–	[208]
Defect effect	Cu$_3$N	0.1 M KHCO$_3$	60	−1.6	30	CP	Flow-cell	20	[178]
	F-Cu	2.5 M KOH	60	−0.54	800	CP	Flow-cell	40	[39]
	Cu$_2$S/Cu-V	1 M KHCO$_3$	21.1	−0.95	–	–	H-cell	–	[172]
Surface modification	C/Cu/PTFE	0.5 M KHCO$_3$ + 0.5 M KCl	70	−0.89	350	PTFE	Flow-cell	50	[109]
	Hydrophobic Cu dendrite	0.1 M CsHCO$_3$	56	-	–	–	H-cell	–	[32]
	Cu-KOH	1 M KOH	54.5	3.25	153	–	MEA	6	[209]
	Cu:Py:SSC	3 M KOH	65	2.6	150	PTFE	MEA	110	[210]
	MgAl-LDH/ Cu	1 M KHCO$_3$	55.1	–	–	CP	Flow-cell	7	[211]

Table 1 (continued)

Strategy	Catalyst	Electrolyte	FE_{C2H4} (%)	E (V vs RHE)	j_{C2H4} (mA cm^{-2})	GDE structure	electrochemical cell	durability (h)	Refs.
Valence state	Cu(B)-2	0.1 M KCl	53±1	−1.0	55	–	H-cell	40	[212]
	AN-Cu	1 M $KHCO_3$	38.1	−1.08	7.3	–	H-cell	40	[213]
	Oxide-derived Cu	0.1 M $KHCO_3$	60	−0.9	–	–	H-cell	–	[214]
	$P_{0.075}$-Cu	0.1 M $KHCO_3$	30.7±0.9	−1.6	17.57	–	H-cell	25	[215]
	Cu-CuI	1 M KOH	71	−0.87	276	–	Flow-cell	85	[216]
	Cu-SiO_x-2.5	0.1 M $KHCO_3$	65	−4.1	215	PTFE	MEA	50	[180]

5.1 Full Mechanistic Picture

The multiple electrons/protons transfer and a large number of reaction intermediates make CO_2RR process extremely complicated [17]. Moreover, the catalytic activity and selectivity of CO_2RR are related to many parameters, such as the catalyst structure and composition (facet, defects, etc.) and reaction conditions (pH, applied potential, electrolyte, etc.), making it even more difficult to achieve the desired products due to the competitions between different reaction pathways. Moreover, the competing HER also decreases the total production of ethylene. It is difficult to suppress H_2 evolution since *H is necessary for CO_2RR mechanism. The selective effect of secondary metals with different binding strengths for *H and *O is vital to alter the products [217]. When secondary metals with weak *H and *O binding energy (such as Ag, Au) form bimetallic catalysts with Cu, due to the synergistic influence of the electronic and geometric effects of the alloy, the weak adsorption energy to *CO is caused, which is facilitates C–C coupling [218]. And weak *H binding also inhibits HER and improves the overall CO_2 utilization rate. Therefore, selecting a secondary metal with an appropriate binding energy of the intermediates can promote the production of ethylene.

5.2 Stability Issues

In addition to the catalytic activity and selectivity for CO_2RR to generate ethylene products, stability is also important to evaluate the catalytic capability of CO_2RR electrocatalysts [219]. Currently, most catalysts can only last less than a few hundred hours under operation conditions. This is far from satisfactory in terms of the practical applications of CO_2RR technologies. Most reports focus on the current density and product selectivity, whereas the stability of catalysts has not received enough attention. Finding a key point to balance the relationship between catalytic activity and stability is desired. Moreover, the degradation mechanisms and corresponding solutions for enhancing the stability of catalysts are needed. Wrapping or embedding Cu-based catalysts in ultrathin layers or anchoring Cu-based materials on stable substrates may achieve excellent stability with no sacrifice for the catalytic activity.

5.3 Operando/In-Situ Techniques and DFT Calculation

Operando/in-situ techniques and DFT calculation are effective tools for understanding the structure-performance relationship [220]. Structure evolution of the catalysts may occur in the CO_2RR conditions, and the operando/in-situ characterization techniques could monitor the dynamic process to identify the real active sites. Moreover, the intermediates can also be detected in real-time for specific reaction pathways. DFT calculation is a powerful tool for acquiring the reaction-free energy of CO_2RR for specific products, revealing the adsorption energies of intermediates and providing an in-depth understanding of the catalytic mechanism at the atomic level. Future efforts may pave the direction of enhancing the time and spatial resolution of operando characterization, and conducting machine-learning coupled DFT to in-depth explore the catalytic mechanism and predict the efficient electrocatalysts.

5.4 Designing Advanced Electrolyzers

Other than the designed catalysts and mechanism understanding of CO_2RR, electrolyzers are also important in practical applications [221–224]. Currently, H-cells are the most widely used devices for CO_2RR, owing to their low cost and simple setup [50]. However, the limited solubility and diffusion of CO_2 in conventional H-cell electrolytes lead to low current densities (< 100 mA cm^{-2}) which limits their commercialization [5, 55, 225]. Therefore, H-cells are usually used in the laboratory for preliminary performance tests. Flow cell is another conventional electrolysis cell. Different from H-cell, CO_2 flows continuously from the back to the catalyst surface through the gas diffusion layer (GDL). Within the flow cell, the rich three-phase boundary composed of CO_2, catalyst and electrolyte significantly improve the reaction efficiency [50, 59, 135]. The advantages of a short CO_2 diffusion path and no solubility limitation strengthen the mass transfer of CO_2, thereby improving the current density and selectivity [59]. However, conventional hydrophobic carbon-based GDL faces the problem of being flooded after a few hours of testing, resulting in flow cell failure. Modification using porous polytetrafluoroethylene (PTFE) as GDL can greatly improve the hydrophobicity and stability of flow cells [29, 226]. However, it is still severe that the reaction of CO_2 with alkaline electrolyte to form carbonate will also lead to low single-pass utilization of CO_2 and the reduction of local pH [55]. Membrane electrode assemblies (MEAs) remove the catholyte and allow the direct contact between the cathode GDL with the exchange membrane, thereby reducing the resistance of the entire cell. Compared to flow cell, MEAs show higher activity and lower energy consumption [14]. However, they still face problems such as low ionic conductivity and low CO_2 utilization ($< 10\%$). Therefore, additional efforts should be made to improve the ionic conductivity and assembly process of ion exchange membranes in the future [55].

Declarations

References

1. Y.H. Fu, D.R. Sun, Y.J. Chen, R.K. Huang, Z.X. Ding et al., An amine-functionalized titanium metal-organic framework photocatalyst with visible-light-induced activity for CO_2 reduction. Angew. Chem. Int. Ed. **51**(14), 3364–3367 (2012). https://doi.org/10.1002/anie.201108357

2. K. Caldeira, M.E. Wickett, Anthropogenic carbon and ocean pH. Nature **425**(6956), 365–365 (2003). https://doi.org/10.1038/425365a

3. V. Masson-Delmotte, M. Kageyama, P. Braconnot, S. Charbit, G. Krinner et al., Past and future polar amplification of climate change: climate model intercomparisons and ice-core constraints. Clim. Dynam. **27**(4), 437–440 (2006). https://doi.org/10.1007/s00382-006-0149-1

4. J.W.C. White, P. Ciais, R.A. Figge, R. Kenny, V. Markgraf, A high-resolution record of atmospheric CO_2 content from carbon isotopes in pet. Nature **367**(6459), 153–156 (1994). https://doi.org/10.1038/367153a0

5. S. Nitopi, E. Bertheussen, S.B. Scott, X.Y. Liu, A.K. Engstfeld et al., Progress and perspectives of electrochemical CO_2 reduction on copper in aqueous electrolyte. Chem. Rev. **119**(12), 7610–7672 (2019). https://doi.org/10.1021/acs.chemrev.8b00705

6. J. Huo, Z. Shen, X. Cao, L. Li, Y. Zhao et al., Macro/microenvironment regulating carbon-supported single-atom catalysts for hydrogen/oxygen conversion reactions. Small **18**(32), 2202394 (2022). https://doi.org/10.1002/smll.202202394

7. J. Huo, X. Cao, Y. Tian, L. Li, J. Qu et al., Atomically dispersed mn atoms coordinated with n and o within an n-doped porous carbon framework for boosted oxygen reduction catalysis. Nanoscale **15**(11), 5448–5457 (2023). https://doi.org/10.1039/D2NR06096E

8. S.M. Benson, F.M. Orr, Carbon dioxide capture and storage. MRS Bull. **33**(4), 303–305 (2008). https://doi.org/10.1557/mrs2008.63

9. G.B. Wen, B.H. Ren, Y. Zheng, M. Li, C. Silva et al., Engineering electrochemical surface for efficient carbon dioxide upgrade. Adv. Energy Mater. **12**(3), 2103289 (2022). https://doi.org/10.1002/aenm.202103289

10. X. Li, J. Wang, X. Lv, Y. Yang, Y. Xu et al., Hetero-interfaces on Cu electrode for enhanced electrochemical conversion of CO_2 to multi-carbon products. Nano-Micro Lett. **14**(1), 134 (2022). https://doi.org/10.1007/s40820-022-00879-5

11. D. Xue, H. Xia, W. Yan, J. Zhang, S. Mu, Defect engineering on carbon-based catalysts for electrocatalytic CO_2 reduction. Nano-Micro Lett. **13**(1), 5 (2020). https://doi.org/10.1007/s40820-020-00538-7

12. C. Qiu, K. Qian, J. Yu, M. Sun, S. Cao et al., MOF-transformed In_2O_{3-x}@C nanocorn electrocatalyst for efficient CO_2 reduction to HCOOH. Nano-Micro Lett. **14**(1), 167 (2022). https://doi.org/10.1007/s40820-022-00913-6

13. C. Ban, Y. Duan, Y. Wang, J. Ma, K. Wang et al., Isotype heterojunction-boosted CO_2 photoreduction to CO. Nano-Micro Lett. **14**(1), 74 (2022). https://doi.org/10.1007/s40820-022-00821-9

14. F.W. Li, A. Thevenon, A. Rosas-Hernandez, Z.Y. Wang, Y.L. Li et al., Molecular tuning of CO_2-to-ethylene conversion. Nature **577**(7791), 509–513 (2020). https://doi.org/10.1038/s41586-019-1782-2

15. P. De Luna, C. Hahn, D. Higgins, S.A. Jaffer, T.F. Jaramillo et al., What would it take for renewably powered electrosynthesis to displace petrochemical processes? Science **364**(6482), 6438 (2020). https://doi.org/10.1126/science.abb0992

16. N. Han, P. Ding, L. He, Y. Li, Y. Li, Promises of main group metal–based nanostructured materials for electrochemical CO_2 reduction to formate. Adv. Energy Mater. **10**(11), 1902338 (2020). https://doi.org/10.1002/aenm.201902338

17. T.K. Todorova, M.W. Schreiber, M. Fontecave, Mechanistic understanding of CO_2 reduction reaction (CO_2RR) toward multicarbon products by heterogeneous copper-based catalysts. ACS Catal. **10**(3), 1754–1768 (2020). https://doi.org/10.1021/acscatal.9b04746

18. X. Cao, J. Huo, L. Li, J. Qu, Y. Zhao et al., Recent advances in engineered Ru-based electrocatalysts for the hydrogen/oxygen conversion reactions. Adv. Energy Mater. **12**(41), 2202119 (2022). https://doi.org/10.1002/aenm.202202119

19. Y. Zhao, J. Zhang, X. Guo, X. Cao, S. Wang et al., Engineering strategies and active site identification of mxene-based catalysts for electrochemical conversion reactions. Chem. Soc. Rev. **52**(9), 3215–3264 (2023). https://doi.org/10.1039/D2CS00698G

20. Y. Hori, K. Kikuchi, A. Murata, S. Suzuki, Production of methane and ethylene in electrochemical reduction of carbon dioxide at copper electrode in aqueous hydrogencarbonate solution. Chem. Lett. **15**(6), 897–898 (1986). https://doi.org/10.1246/cl.1986.897

21. Y. Hori, A. Murata, R. Takahashi, Formation of hydrocarbons in the electrochemical reduction of carbon dioxide at a copper electrode in aqueous solution. J. Chem. Soc. Faraday Transl. **85**(8), 2309–2326 (1989). https://doi.org/10.1039/F19898502309

22. Y. Hori, A. Murata, R. Takahashi, S. Suzuki, Electroreduction of carbon monoxide to methane and ethylene at a copper electrode in aqueous solutions at ambient temperature and pressure. J. Am. Chem. Soc. **109**, 5022–5023 (1987). https://doi.org/10.1021/ja00250a044

23. Y. Hori, A. Murata, R. Takahashi, S. Suzuki, Enhanced formation of ethylene and alcohols at ambient temperature and pressure in electrochemical reduction of carbon dioxide at a copper electrode. J. Chem. Soc. Chem. Commun. **1**, 17–19 (1988). https://doi.org/10.1039/C39880000017

24. H. Yoshio, M. Akira, T. Ryutaro, S. Shin, Electrochemical reduction of carbon monoxide to hydrocarbons at various metal electrodes in aqueous solution. Chem. Lett. **16**(8), 1665–1668 (1987). https://doi.org/10.1246/cl.1987.1665

25. B.X. Zhang, J.L. Zhang, M.L. Hua, Q. Wan, Z.Z. Su et al., Highly electrocatalytic ethylene production from CO_2 on nanodefective Cu nanosheets. J. Am. Chem. Soc. **142**(31), 13606–13613 (2020). https://doi.org/10.1021/jacs.0c06420

26. M.G. Kibria, C.T. Dinh, A. Seifitokaldani, P. De Luna, T. Burdyny et al., A surface reconstruction route to high productivity and selectivity in CO_2 electroreduction toward C_{2+} hydrocarbons. Adv. Mater. **30**(49), 1804867 (2018). https://doi.org/10.1002/adma.201804867

27. C. Choi, S. Kwon, T. Cheng, M.J. Xu, P. Tieu et al., Highly active and stable stepped Cu surface for enhanced electrochemical CO_2 reduction to C_2H_4. Nat. Catal. **3**(10), 804–812 (2020). https://doi.org/10.1038/s41929-020-00504-x

28. Y. Chen, Z.X. Fan, J. Wang, C.Y. Ling, W.X. Niu et al., Ethylene selectivity in electrocatalytic CO_2 reduction on cu nanomaterials: a crystal phase-dependent study. J. Am. Chem. Soc. **142**(29), 12760–12766 (2020). https://doi.org/10.1021/jacs.0c04981

29. C.T. Dinh, T. Burdyny, M.G. Kibria, A. Seifitokaldani, C.M. Gabardo et al., CO_2 electroreduction to ethylene via hydroxide-mediated copper catalysis at an abrupt interface. Science **360**(6390), 783–787 (2018). https://doi.org/10.1126/science.aas9100

30. M. Zhong, K. Tran, Y.M. Min, C.H. Wang, Z.Y. Wang et al., Accelerated discovery of CO_2 electrocatalysts using active machine learning. Nature **581**(7807), 178–183 (2020). https://doi.org/10.1038/s41586-020-2242-8

31. J.J. Wu, S.C. Ma, J. Sun, J.I. Gold, C. Tiwary et al., A metal-free electrocatalyst for carbon dioxide reduction to multi-carbon hydrocarbons and oxygenates. Nat. Commun. **7**, 13869 (2016). https://doi.org/10.1038/ncomms13869

32. D. Wakerley, S. Lamaison, F. Ozanam, N. Menguy, D. Mercier et al., Bio-inspired hydrophobicity promotes CO_2 reduction on a Cu surface. Nat. Mater. **18**(11), 1222–1227 (2019). https://doi.org/10.1038/s41563-019-0445-x

33. D.H. Nam, O.S. Bushuyev, J. Li, P. De Luna, A. Seifitokaldani et al., Metal-organic frameworks mediate Cu coordination for selective CO_2 electroreduction. J. Am. Chem. Soc. **140**(36), 11378–11386 (2018). https://doi.org/10.1021/jacs.8b06407

34. N. Martic, C. Reller, C. Macauley, M. Loffler, B. Schmid et al., Paramelaconite-enriched copper-based material as an efficient and robust catalyst for electrochemical carbon dioxide reduction. Adv. Energy Mater. **9**(29), 1901228 (2019). https://doi.org/10.1002/aenm.201901228

35. J. Kim, W. Choi, J.W. Park, C. Kim, M. Kim et al., Branched copper oxide nanoparticles induce highly selective ethylene production by electrochemical carbon dioxide reduction. J. Am. Chem. Soc. **141**(17), 6986–6994 (2019). https://doi.org/10.1021/jacs.9b00911

36. B. Yang, K. Liu, H. Li, C. Liu, J. Fu et al., Accelerating CO_2 electroreduction to multicarbon products via synergistic electric-thermal field on copper nanoneedles. J. Am. Chem. Soc. **144**(7), 3039–3049 (2022). https://doi.org/10.1021/jacs.1c11253

37. D.-H. Nam, O. Shekhah, A. Ozden, C. McCallum, F. Li et al., High-rate and selective CO_2 electrolysis to ethylene via metal-organic-framework-augmented CO_2 availability. Adv. Mater. **34**(51), 2207088 (2022). https://doi.org/10.1002/adma.202207088

38. J. Zhang, Y. Wang, Z. Li, S. Xia, R. Cai et al., Grain boundary-derived Cu^+/Cu^0 interfaces in CuO nanosheets for low overpotential carbon dioxide electroreduction to ethylene. Adv. Sci. **9**(21), 2200454 (2022). https://doi.org/10.1002/advs.202200454

39. W.C. Ma, S.J. Xie, T.T. Liu, Q.Y. Fan, J.Y. Ye et al., Electrocatalytic reduction of CO_2 to ethylene and ethanol through hydrogen-assisted C–C coupling over fluorine-modified copper. Nat. Catal. **3**(6), 478–487 (2020). https://doi.org/10.1038/s41929-020-0450-0

40. A.J. Garza, A.T. Bell, M. Head-Gordon, Mechanism of CO_2 reduction at copper surfaces: pathways to C_2 products. ACS Catal. **8**(2), 1490–1499 (2018). https://doi.org/10.1021/acscatal.7b03477

41. Y.W. Lum, T. Cheng, W.A. Goddard, J.W. Ager, Electrochemical CO reduction builds solvent water into oxygenate products. J. Am. Chem. Soc. **140**(30), 9337–9340 (2018). https://doi.org/10.1021/jacs.8b03986

42. F. Calle-Vallejo, M.T. Koper, Theoretical considerations on the electroreduction of CO to C_2 species on Cu(100) electrodes. Angew. Chem. Int. Ed. **52**(28), 7282–7285 (2013). https://doi.org/10.1002/anie.201301470

43. M.B. Ross, P. De Luna, Y.F. Li, C.T. Dinh, D. Kim et al., Designing materials for electrochemical carbon dioxide recycling. Nat. Catal. **2**(8), 648–658 (2019). https://doi.org/10.1038/s41929-019-0306-7

44. M.R. Singh, E.L. Clark, A.T. Bell, Effects of electrolyte, catalyst, and membrane composition and operating conditions on the performance of solar-driven electrochemical reduction of carbon dioxide. Phys. Chem. Chem. Phys. **17**(29), 18924–18936 (2015). https://doi.org/10.1039/c5cp03283k

45. L.M. Wang, W.L. Chen, D.D. Zhang, Y.P. Du, R. Amal et al., Surface strategies for catalytic CO_2 reduction: from two-dimensional materials to nanoclusters to single atoms. Chem. Soc. Rev. **48**(21), 5310–5349 (2019). https://doi.org/10.1039/c9cs00163h

46. G. Zhang, Z.-J. Zhao, D. Cheng, H. Li, J. Yu et al., Efficient CO_2 electroreduction on facet-selective copper films with high conversion rate. Nat. Commun. **12**(1), 5745 (2021). https://doi.org/10.1038/s41467-021-26053-w

47. X.X. Chang, T. Wang, J.L. Gong, CO_2 photo-reduction: insights into CO_2 activation and reaction on surfaces of photocatalysts. Energy Environ. Sci. **9**(7), 2177–2196 (2016). https://doi.org/10.1039/c6ee00383d

48. M. Favaro, H. Xiao, T. Cheng, W.A. Goddard, J. Yano et al., Subsurface oxide plays a critical role in CO_2 activation by Cu(111) surfaces to form chemisorbed CO_2, the first step in reduction of CO_2. Proc. Natl. Acad. Sci. **114**(26), 6706–6711 (2017). https://doi.org/10.1073/pnas.1701405114

49. Z.Y. Sun, T. Ma, H.C. Tao, Q. Fan, B.X. Han, Fundamentals and challenges of electrochemical CO_2 reduction using two-dimensional materials. Chem **3**(4), 560–587 (2017). https://doi.org/10.1016/j.chempr.2017.09.009

50. Y. Yang, Z. Tan, J. Zhang, Electrocatalytic carbon dioxide reduction to ethylene over copper-based catalytic systems. Chem. Asian J. **17**(24), e202200893 (2022). https://doi.org/10.1002/asia.202200893

51. M. Zheng, P. Wang, X. Zhi, K. Yang, Y. Jiao et al., Electrocatalytic CO_2-to-C_{2+} with ampere-level current on heteroatom-engineered copper via tuning *CO intermediate coverage. J. Am. Chem. Soc. **144**(32), 14936–14944 (2022). https://doi.org/10.1021/jacs.2c06820

52. J. Hou, X. Chang, J. Li, B. Xu, Q. Lu, Correlating CO coverage and CO electroreduction on Cu via high-pressure in situ spectroscopic and reactivity investigations. J. Am. Chem. Soc. **144**(48), 22202–22211 (2022). https://doi.org/10.1021/jacs.2c09956

53. Y. Kim, S. Park, S.J. Shin, W. Choi, B.K. Min et al., Time-resolved observation of C–C coupling intermediates on Cu electrodes for selective electrochemical CO_2 reduction. Energy Environ. Sci. **13**(11), 4301–4311 (2020). https://doi.org/10.1039/d0ee01690j

54. E. Pérez-Gallent, M.C. Figueiredo, F. Calle-Vallejo, M.T.M. Koper, Spectroscopic observation of a hydrogenated CO dimer intermediate during CO reduction on Cu(100) electrodes. Angew. Chem. Int. Ed. **56**(13), 3621–3624 (2017). https://doi.org/10.1002/anie.201700580

55. W.C. Ma, X.Y. He, W. Wang, S.J. Xie, Q.H. Zhang et al., Electrocatalytic reduction of CO_2 and CO to multi-carbon compounds over Cu-based catalysts. Chem. Soc. Rev.

50(23), 12897–12914 (2021). https://doi.org/10.1039/d1cs00535a

56. T. Cheng, H. Xiao, W.A. Goddard, Full atomistic reaction mechanism with kinetics for CO reduction on Cu(100) from ab initio molecular dynamics free-energy calculations at 298 k. Proc. Natl. Acad. Sci. **114**(8), 1795–1800 (2017). https://doi.org/10.1073/pnas.1612106114

57. J.D. Goodpaster, A.T. Bell, M. Head-Gordon, Identification of possible pathways for C–C bond formation during electrochemical reduction of CO_2: new theoretical insights from an improved electrochemical model. J. Phys. Chem. Lett. **7**(8), 1471–1477 (2016). https://doi.org/10.1021/acs.jpclett.6b00358

58. H. Xiao, T. Cheng, W.A. Goddard, Atomistic mechanisms underlying selectivities in C_1 and C_2 products from electrochemical reduction of CO on Cu(111). J. Am. Chem. Soc. **139**(1), 130–136 (2017). https://doi.org/10.1021/jacs.6b06846

59. Y.H. Wang, J.L. Liu, G.F. Zheng, Designing copper-based catalysts for efficient carbon dioxide electroreduction. Adv. Mater. **33**(46), 2005798 (2021). https://doi.org/10.1002/adma.202005798

60. Z. Ni, H. Liang, Z. Yi, R. Guo, C. Liu et al., Research progress of electrochemical CO_2 reduction for copper-based catalysts to multicarbon products. Coordin. Chem. Rev. **441**, 213983 (2021). https://doi.org/10.1016/j.ccr.2021.213983

61. Y. Hori, H. Wakebe, T. Tsukamoto, O. Koga, Electrocatalytic process of CO selectivity in electrochemical reduction of CO_2 at metal electrodes in aqueous media. Electrochim. Acta **39**(11), 1833–1839 (1994). https://doi.org/10.1016/0013-4686(94)85172-7

62. Y. Hori, R. Takahashi, Y. Yoshinami, A. Murata, Electrochemical reduction of CO at a copper electrode. J. Phys. Chem. B **101**(36), 7075–7081 (1997). https://doi.org/10.1021/jp970284i

63. A.A. Peterson, F. Abild-Pedersen, F. Studt, J. Rossmeisl, J.K. Norskov, How copper catalyzes the electroreduction of carbon dioxide into hydrocarbon fuels. Energy Environ. Sci. **3**(9), 1311–1315 (2010). https://doi.org/10.1039/c0ee00071j

64. K.P. Kuhl, E.R. Cave, D.N. Abram, T.F. Jaramillo, New insights into the electrochemical reduction of carbon dioxide on metallic copper surfaces. Energy Environ. Sci. **5**(5), 7050–7059 (2012). https://doi.org/10.1039/c2ee21234j

65. J.H. Montoya, C. Shi, K. Chan, J.K. Norskov, Theoretical insights into a CO dimerization mechanism in CO_2 electroreduction. J. Phys. Chem. Lett. **6**(11), 2032–2037 (2015). https://doi.org/10.1021/acs.jpclett.5b00722

66. R. Kortlever, J. Shen, K.J.P. Schouten, F. Calle-Vallejo, M.T.M. Koper, Catalysts and reaction pathways for the electrochemical reduction of carbon dioxide. J. Phys. Chem. Lett. **6**(20), 4073–4082 (2015). https://doi.org/10.1021/acs.jpclett.5b01559

67. T. Cheng, H. Xiao, W.A. Goddard, Free-energy barriers and reaction mechanisms for the electrochemical reduction of CO on the Cu(100) surface, including multiple layers of explicit solvent at pH 0. J. Phys. Chem. Lett. **6**(23), 4767–4773 (2015). https://doi.org/10.1021/acs.jpclett.5b02247

68. J.T. Feaster, C. Shi, E.R. Cave, T.T. Hatsukade, D.N. Abram et al., Understanding selectivity for the electrochemical reduction of carbon dioxide to formic acid and carbon monoxide on metal electrodes. ACS Catal. **7**(7), 4822–4827 (2017). https://doi.org/10.1021/acscatal.7b00687

69. X. Liu, P. Schlexer, J. Xiao, Y. Ji, L. Wang et al., pH effects on the electrochemical reduction of CO_2 towards C_2 products on stepped copper. Nat. Commun. **10**(1), 32 (2019). https://doi.org/10.1038/s41467-018-07970-9

70. I.V. Chernyshova, P. Somasundaran, S. Ponnurangam, On the origin of the elusive first intermediate of CO_2 electroreduction. Proc. Natl. Acad. Sci. **115**(40), E9261–E9270 (2018). https://doi.org/10.1073/pnas.1802256115

71. S.A. Petrosyan, A.A. Rigos, T.A. Arias, Joint density-functional theory: Ab initio study of Cr_2O_3 surface chemistry in solution. J. Phys. Chem. B **109**(32), 15436–15444 (2005). https://doi.org/10.1021/jp044822k

72. R. Sundararaman, W.A. Goddard, The charge-asymmetric nonlocally determined local-electric (candle) solvation model. J. Chem. Phys. **142**(6), 064107 (2015). https://doi.org/10.1063/1.4907731

73. X.W. Nie, M.R. Esopi, M.J. Janik, A. Asthagiri, Selectivity of CO_2 reduction on copper electrodes: the role of the kinetics of elementary steps. Angew. Chem. Int. Ed. **52**(9), 2459–2462 (2013). https://doi.org/10.1002/anie.201208320

74. X.W. Nie, W.J. Luo, M.J. Janik, A. Asthagiri, Reaction mechanisms of CO_2 electrochemical reduction on Cu(111) determined with density functional theory. J. Catal. **312**, 108–122 (2014). https://doi.org/10.1016/j.jcat.2014.01.013

75. K.J.P. Schouten, Y. Kwon, C.J.M. van der Ham, Z. Qin, M.T.M. Koper, A new mechanism for the selectivity to C_1 and C_2 species in the electrochemical reduction of carbon dioxide on copper electrodes. Chem. Sci. **2**(10), 1902–1909 (2011). https://doi.org/10.1039/c1sc00277e

76. F.S. Roberts, K.P. Kuhl, A. Nilsson, High selectivity for ethylene from carbon dioxide reduction over copper nanocube electrocatalysts. Angew. Chem. Int. Ed. **54**(17), 5179–5182 (2015). https://doi.org/10.1002/anie.201412214

77. H. Xiao, T. Cheng, W.A. Goddard, R. Sundararaman, Mechanistic explanation of the ph dependence and onset potentials for hydrocarbon products from electrochemical reduction of CO on Cu (111). J. Am. Chem. Soc. **138**(2), 483–486 (2016). https://doi.org/10.1021/jacs.5b11390

78. Y.Y. Birdja, E. Pérez-Gallent, M.C. Figueiredo, A.J. Göttle, F. Calle-Vallejo et al., Advances and challenges in understanding the electrocatalytic conversion of carbon dioxide to fuels. Nat. Energy **4**(9), 732–745 (2019). https://doi.org/10.1038/s41560-019-0450-y

79. B. Pan, Y. Wang, Y. Li, Understanding and leveraging the effect of cations in the electrical double layer for electrochemical CO_2 reduction. Chem. Catal. **2**(6), 1267–1276 (2022). https://doi.org/10.1016/j.checat.2022.03.012

80. B. Endrődi, G. Bencsik, F. Darvas, R. Jones, K. Rajeshwar et al., Continuous-flow electroreduction of carbon dioxide.

Prog. Energy Combust. Sci. **62**, 133–154 (2017). https://doi.org/10.1016/j.pecs.2017.05.005

81. C. Chen, J.F. Khosrowabadi Kotyk, S.W. Sheehan, Progress toward commercial application of electrochemical carbon dioxide reduction. Chem **4**(11), 2571–2586 (2018). https://doi.org/10.1016/j.chempr.2018.08.019

82. W. Nie, G.P. Heim, N.B. Watkins, T. Agapie, J.C. Peters, Organic additive-derived films on Cu electrodes promote electrochemical CO_2 reduction to C_{2+} products under strongly acidic conditions. Angew. Chem. Int. Ed. **62**(12), e202216102 (2023). https://doi.org/10.1002/anie.202216102

83. M. Ma, K. Djanashvili, W.A. Smith, Controllable hydrocarbon formation from the electrochemical reduction of CO_2 over Cu nanowire arrays. Angew. Chem. Int. Ed. **55**(23), 6680–6684 (2016). https://doi.org/10.1002/anie.201601282

84. T. Ahmad, S. Liu, M. Sajid, K. Li, M. Ali et al., Electrochemical CO_2 reduction to C_{2+} products using Cu-based electrocatalysts: a review. Nano Res. Energy **1**, e9120021 (2022). https://doi.org/10.26599/NRE.2022.9120021

85. M.C.O. Monteiro, F. Dattila, B. Hagedoorn, R. García-Muelas, N. López et al., Absence of CO_2 electroreduction on copper, gold and silver electrodes without metal cations in solution. Nat. Catal. **4**(8), 654–662 (2021). https://doi.org/10.1038/s41929-021-00655-5

86. A. Murata, Y. Hori, Product selectivity affected by cationic species in electrochemical reduction of CO_2 and CO at a Cu electrode. B Chem. Soc. of Jpn. **64**(1), 123–127 (1991). https://doi.org/10.1246/bcsj.64.123

87. E. Pérez-Gallent, G. Marcandalli, M.C. Figueiredo, F. Calle-Vallejo, M.T.M. Koper, Structure- and potential-dependent cation effects on CO reduction at copper single-crystal electrodes. J. Am. Chem. Soc. **139**(45), 16412–16419 (2017). https://doi.org/10.1021/jacs.7b10142

88. J. Resasco, L.D. Chen, E. Clark, C. Tsai, C. Hahn et al., Promoter effects of alkali metal cations on the electrochemical reduction of carbon dioxide. J. Am. Chem. Soc. **139**(32), 11277–11287 (2017). https://doi.org/10.1021/jacs.7b06765

89. V.J. Ovalle, Y.-S. Hsu, N. Agrawal, M.J. Janik, M.M. Waegele, Correlating hydration free energy and specific adsorption of alkali metal cations during CO_2 electroreduction on Au. Nat. Catal. **5**(7), 624–632 (2022). https://doi.org/10.1038/s41929-022-00816-0

90. H. Liu, J. Liu, B. Yang, Promotional role of a cation intermediate complex in C_2 formation from electrochemical reduction of CO_2 over Cu. ACS Catal. **11**(19), 12336–12343 (2021). https://doi.org/10.1021/acscatal.1c01072

91. A.S. Malkani, J. Li, N.J. Oliveira, M. He, X. Chang et al., Understanding the electric and nonelectric field components of the cation effect on the electrochemical CO reduction reaction. Sci. Adv. **6**(45), eabd2569 (2020). https://doi.org/10.1126/sciadv.abd2569

92. M.R. Singh, Y. Kwon, Y. Lum, J.W. Ager III., A.T. Bell, Hydrolysis of electrolyte cations enhances the electrochemical reduction of CO_2 over Ag and Cu. J. Am. Chem. Soc. **138**(39), 13006–13012 (2016). https://doi.org/10.1021/jacs.6b07612

93. O. Ayemoba, A. Cuesta, Spectroscopic evidence of size-dependent buffering of interfacial ph by cation hydrolysis during CO_2 electroreduction. ACS Appl. Mater. Interfaces **9**(33), 27377–27382 (2017). https://doi.org/10.1021/acsami.7b07351

94. F. Zhang, A.C. Co, Direct evidence of local pH change and the role of alkali cation during CO_2 electroreduction in aqueous media. Angew. Chem. Int. Ed. **59**(4), 1674–1681 (2020). https://doi.org/10.1002/anie.201912637

95. G. Marcandalli, M.C.O. Monteiro, A. Goyal, M.T.M. Koper, Electrolyte effects on CO_2 electrochemical reduction to CO. Accounts Chem. Res. **55**(14), 1900–1911 (2022). https://doi.org/10.1021/acs.accounts.2c00080

96. K.J.P. Schouten, E. Pérez Gallent, M.T.M. Koper, The influence of pH on the reduction of CO and CO_2 to hydrocarbons on copper electrodes. J. Electroanaly. Chem. **716**, 53–57 (2014). https://doi.org/10.1016/j.jelechem.2013.08.033

97. A.S. Varela, M. Kroschel, T. Reier, P. Strasser, Controlling the selectivity of CO_2 electroreduction on copper: the effect of the electrolyte concentration and the importance of the local pH. Catal. Today **260**, 8–13 (2016). https://doi.org/10.1016/j.cattod.2015.06.009

98. Y. Zheng, A. Vasileff, X. Zhou, Y. Jiao, M. Jaroniec et al., Understanding the roadmap for electrochemical reduction of CO_2 to multi-carbon oxygenates and hydrocarbons on copper-based catalysts. J. Am. Chem. Soc. **141**(19), 7646–7659 (2019). https://doi.org/10.1021/jacs.9b02124

99. K. Jiang, R.B. Sandberg, A.J. Akey, X. Liu, D.C. Bell et al., Metal ion cycling of Cu foil for selective C–C coupling in electrochemical CO_2 reduction. Nat. Catal. **1**(2), 111–119 (2018). https://doi.org/10.1038/s41929-017-0009-x

100. D. Gao, R.M. Arán-Ais, H.S. Jeon, B. Roldan Cuenya, Rational catalyst and electrolyte design for CO_2 electroreduction towards multicarbon products. Nat. Catal. **2**(3), 198–210 (2019). https://doi.org/10.1038/s41929-019-0235-5

101. G. Chen, J. Fu, B. Liu, C. Cai, H. Li et al., Passivation of Cu nanosheet dissolution with Cu^{2+}-containing electrolytes for selective electroreduction of CO_2 to CH_4. Environ. Sci-Nano **9**(9), 3312–3317 (2022). https://doi.org/10.1039/D2EN00561A

102. J. Li, Z.Y. Wang, C. McCallum, Y. Xu, F.W. Li et al., Constraining CO coverage on copper promotes high-efficiency ethylene electroproduction. Nat. Catal. **2**(12), 1124–1131 (2019). https://doi.org/10.1038/s41929-019-0380-x

103. K.J.P. Schouten, E. Pérez Gallent, M.T.M. Koper, Structure sensitivity of the electrochemical reduction of carbon monoxide on copper single crystals. ACS Catal. **3**(6), 1292–1295 (2013). https://doi.org/10.1021/cs4002404

104. D. Wakerley, S. Lamaison, J. Wicks, A. Clemens, J. Feaster et al., Gas diffusion electrodes, reactor designs and key metrics of low-temperature CO_2 electrolysers. Nat. Energy **7**(2), 130–143 (2022). https://doi.org/10.1038/s41560-021-00973-9

105. D.M. Weekes, D.A. Salvatore, A. Reyes, A. Huang, C.P. Berlinguette, Electrolytic CO_2 reduction in a flow cell. Acc.

Chem. Res. **51**(4), 910–918 (2018). https://doi.org/10.1021/acs.accounts.8b00010

106. X. Zhou, H. Liu, B.Y. Xia, K. Ostrikov, Y. Zheng et al., Customizing the microenvironment of CO_2 electrocatalysis via three-phase interface engineering. SmartMat **3**(1), 111–129 (2022). https://doi.org/10.1002/smm2.1109

107. A.K. Buckley, M. Lee, T. Cheng, R.V. Kazantsev, D.M. Larson et al., Electrocatalysis at organic-metal interfaces: Identification of structure-reactivity relationships for CO_2 reduction at modified Cu surfaces. J. Am. Chem. Soc. **141**(18), 7355–7364 (2019). https://doi.org/10.1021/jacs.8b13655

108. H. Noda, S. Ikeda, Y. Oda, K. Ito, Potential dependencies of the products on electrochemical reduction of carbon dioxide at a copper electrode. Chem. Lett. **18**(2), 289–292 (1989). https://doi.org/10.1246/cl.1989.289

109. Z. Wang, Y. Li, X. Zhao, S. Chen, Q. Nian et al., Localized alkaline environment via in situ electrostatic confinement for enhanced CO_2-to-ethylene conversion in neutral medium. J. Am. Chem. Soc. **145**(11), 6339–6348 (2023). https://doi.org/10.1021/jacs.2c13384

110. F.P. Pan, Y. Yang, Designing CO_2 reduction electrode materials by morphology and interface engineering. Energy Environ. Sci. **13**(8), 2275–2309 (2020). https://doi.org/10.1039/d0ee00900h

111. Y. Xia, Y. Xiong, B. Lim, S.E. Skrabalak, Cover picture: Shape-controlled synthesis of metal nanocrystals: simple chemistry meets complex physics? Angew. Chem. Int. Ed. **48**(1), 90275 (2009). https://doi.org/10.1002/anie.200890275

112. Y.F. Shi, Z.H. Lyu, M. Zhao, R.H. Chen, Q.N. Nguyen et al., Noble-metal nanocrystals with controlled shapes for catalytic and electrocatalytic applications. Chem. Rev. **121**(2), 649–735 (2021). https://doi.org/10.1021/acs.chemrev.0c00454

113. D.H. Chi, H.P. Yang, Y.F. Du, T. Lv, G.J. Sui et al., Morphology-controlled CuO nanoparticles for electroreduction of CO_2 to ethanol. RSC Adv. **4**(70), 37329–37332 (2014). https://doi.org/10.1039/c4ra05415f

114. J.W. Yin, J. Wang, Y.B. Ma, J.L. Yu, J.W. Zhou et al., Recent advances in the controlled synthesis and catalytic applications of two-dimensional rhodium nanomaterials. ACS Mater. Lett. **3**(1), 121–133 (2021). https://doi.org/10.1021/acsmaterialslett.0c00473

115. H.Y. Zhang, Y.J. Zhang, Y.Y. Li, S. Ahn, G.T.R. Palmore et al., Cu nanowire- catalyzed electrochemical reduction of CO or CO_2. Nanoscale **11**(25), 12075–12079 (2019). https://doi.org/10.1039/c9nr03170g

116. Q. Li, W.L. Zhu, J.J. Fu, H.Y. Zhang, G. Wu et al., Controlled assembly of Cu nanoparticles on pyridinic-n rich graphene for electrochemical reduction of CO_2 to ethylene. Nano Energy **24**, 1–9 (2016). https://doi.org/10.1016/j.nanoen.2016.03.024

117. N.T. Suen, Z.R. Kong, C.S. Hsu, H.C. Chen, C.W. Tung et al., Morphology manipulation of copper nanocrystals and product selectivity in the electrocatalytic reduction of carbon dioxide. ACS Catal. **9**(6), 5217–5222 (2019). https://doi.org/10.1021/acscatal.9b00790

118. Z.Y. Chang, S.J. Huo, W. Zhang, J.H. Fang, H.L. Wang, The tunable and highly selective reduction products on Ag@Cu bimetallic catalysts toward CO_2 electrochemical reduction reaction. J. Phys. Chem. C **121**(21), 11368–11379 (2017). https://doi.org/10.1021/acs.jpcc.7b01586

119. J.J. Lv, M. Jouny, W. Luc, W.L. Zhu, J.J. Zhu et al., A highly porous copper electrocatalyst for carbon dioxide reduction. Adv. Mater. **30**(49), 1803111 (2018). https://doi.org/10.1002/adma.201803111

120. Y. Hori, in *Electrochemical CO2 Reduction on Metal Electrodes*. ed. by C.G. Vayenas, R.E. White, M.E. Gamboa-aldeco (Springer, New York, 2008), pp.89–189

121. J.H. Baricuatro, Y.-G. Kim, C.L. Korzeniewski, M.P. Soriaga, *Seriatim* ECSTM-ECPMIRS of the adsorption of carbon monoxide on Cu(100) in alkaline solution at CO_2-reduction potentials. Electrochem. Commun. **91**, 1–4 (2018). https://doi.org/10.1016/j.elecom.2018.04.016

122. W. Liu, P. Zhai, A. Li, B. Wei, K. Si et al., Electrochemical CO_2 reduction to ethylene by ultrathin CuO nanoplate arrays. Nat. Commun. **13**(1), 1877 (2022). https://doi.org/10.1038/s41467-022-29428-9

123. T. Burdyny, P.J. Graham, Y.J. Pang, C.T. Dinh, M. Liu et al., Nanomorphology-enhanced gas-evolution intensifies CO_2 reduction electrochemistry. ACS Sustain. Chem. Eng. **5**(5), 4031–4040 (2017). https://doi.org/10.1021/acssuschemeng.7b00023

124. H. Kakizaki, H. Ooka, T. Hayashi, A. Yamaguchi, N. Bonnet-Mercier et al., Evidence that crystal facet orientation dictates oxygen evolution intermediates on rutile manganese oxide. Adv. Funct. Mater. **28**(24), 1706319 (2018). https://doi.org/10.1002/adfm.201706319

125. T. Wu, M.L. Stone, M.J. Shearer, M.J. Stolt, I.A. Guzei et al., Crystallographic facet dependence of the hydrogen evolution reaction on cops: theory and experiments. ACS Catal. **8**(2), 1143–1152 (2018). https://doi.org/10.1021/acscatal.7b03167

126. S.C. Wang, G. Liu, L.Z. Wang, Crystal facet engineering of photoelectrodes for photoelectrochemical water splitting. Chem. Rev. **119**(8), 5192–5247 (2019). https://doi.org/10.1021/acs.chemrev.8b00584

127. Y. Hori, I. Takahashi, O. Koga, N. Hoshi, Electrochemical reduction of carbon dioxide at various series of copper single crystal electrodes. J. Mol. Catal. A-Chem. **199**(1–2), 39–47 (2003). https://doi.org/10.1016/S1381-1169(03)00016-5

128. Y. Hori, I. Takahashi, O. Koga, N. Hoshi, Selective formation of C_2 compounds from electrochemical reduction of CO_2 at a series of copper single crystal electrodes. J. Phys. Chem. B **106**(1), 15–17 (2002). https://doi.org/10.1021/jp013478d

129. Y. Hori, H. Wakebe, T. Tsukamoto, O. Koga, Adsorption of CO accompanied with simultaneous charge transfer on copper single crystal electrodes related with electrochemical reduction of CO_2 to hydrocarbons. Surf. Sci. **335**, 258–263 (1995). https://doi.org/10.1016/0039-6028(95)00441-6

130. W.J. Luo, X.W. Nie, M.J. Janik, A. Asthagiri, Facet dependence of CO_2 reduction paths on Cu electrodes. ACS Catal. **6**(1), 219–229 (2016). https://doi.org/10.1021/acscatal.5b01967

131. Y. Huang, A.D. Handoko, P. Hirunsit, B.S. Yeo, Electrochemical reduction of CO_2 using copper single-crystal surfaces: effects of *CO coverage on the selective formation of ethylene. ACS Catal. **7**(3), 1749–1756 (2017). https://doi.org/10.1021/acscatal.6b03147

132. G.L. De Gregorio, T. Burdyny, A. Loiudice, P. Iyengar, W.A. Smith et al., Facet-dependent selectivity of Cu catalysts in electrochemical CO_2 reduction at commercially viable current densities. ACS Catal. **10**(9), 4854–4862 (2020). https://doi.org/10.1021/acscatal.0c00297

133. H. Li, P. Yu, R. Lei, F. Yang, P. Wen et al., Facet-selective deposition of ultrathin Al_2O_3 on copper nanocrystals for highly stable CO_2 electroreduction to ethylene. Angew. Chem. Int. Ed. **60**(47), 24838–24843 (2021). https://doi.org/10.1002/anie.202109600

134. C.S. Chen, A.D. Handoko, J.H. Wan, L. Ma, D. Ren et al., Stable and selective electrochemical reduction of carbon dioxide to ethylene on copper mesocrystals. Catal. Sci. Technol. **5**(1), 161–168 (2015). https://doi.org/10.1039/c4cy00906a

135. Y.H. Wang, Z.Y. Wang, C.T. Dinh, J. Li, A. Ozden et al., Catalyst synthesis under CO_2 electroreduction favours faceting and promotes renewable fuels electrosynthesis. Nat. Catal. **3**(2), 98–106 (2020). https://doi.org/10.1038/s41929-019-0397-1

136. H. Luo, B. Li, J.G. Ma, P. Cheng, Surface modification of nano-CuO_2 for controlling CO_2 electrochemical reduction to ethylene and syngas. Angew. Chem. Int. Ed. **61**(11), e202116736 (2022). https://doi.org/10.1002/anie.202116736

137. H. Deng, C. Guo, P. Shi, G. Zhao, Amino assisted protonation for carbon-carbon coupling during electroreduction of carbon dioxide to ethylene on copper(i) oxide. ChemCatChem **13**(20), 4325–4333 (2021). https://doi.org/10.1002/cctc.202100620

138. L. Li, A.H. Larsen, N.A. Romero, V.A. Morozov, C. Glinsvad et al., Investigation of catalytic finite-size-effects of platinum metal clusters. J. Phys. Chem. Lett. **4**(1), 222–226 (2013). https://doi.org/10.1021/jz3018286

139. R. Reske, H. Mistry, F. Behafarid, B. Roldan Cuenya, P. Strasser, Particle size effects in the catalytic electroreduction of CO_2 on Cu nanoparticles. J. Am. Chem. Soc. **136**(19), 6978–6986 (2014). https://doi.org/10.1021/ja500328k

140. A. Loiudice, P. Lobaccaro, E.A. Kamali, T. Thao, B.H. Huang et al., Tailoring copper nanocrystals towards C_2 products in electrochemical CO_2 reduction. Angew. Chem. Int. Ed. **55**(19), 5789–5792 (2016). https://doi.org/10.1002/anie.201601582

141. A.D. Handoko, C.W. Ong, Y. Huang, Z.G. Lee, L.Y. Lin et al., Mechanistic insights into the selective electroreduction of carbon dioxide to ethylene on Cu_2O-derived copper catalysts. J. Phys. Chem. C **120**(36), 20058–20067 (2016). https://doi.org/10.1021/acs.jpcc.6b07128

142. D.H. Nam, P. De Luna, A. Rosas-Hernandez, A. Thevenon, F.W. Li et al., Molecular enhancement of heterogeneous CO_2 reduction. Nat. Mater. **19**(3), 266–276 (2020). https://doi.org/10.1038/s41563-020-0610-2

143. X.F. Li, Q.L. Zhu, Mof-based materials for photo- and electrocatalytic CO_2 reduction. Energychem **2**(3), 100033 (2020). https://doi.org/10.1016/j.enchem.2020.100033

144. J.L. Yu, J. Wang, Y.B. Ma, J.W. Zhou, Y.H. Wang et al., Recent progresses in electrochemical carbon dioxide reduction on copper-based catalysts toward multicarbon products. Adv. Funct. Mater. **31**(37), 2102151 (2021). https://doi.org/10.1002/adfm.202102151

145. Z. Weng, J.B. Jiang, Y.S. Wu, Z.S. Wu, X.T. Guo et al., Electrochemical CO_2 reduction to hydrocarbons on a heterogeneous molecular Cu catalyst in aqueous solution. J. Am. Chem. Soc. **138**(26), 8076–8079 (2016). https://doi.org/10.1021/jacs.6b04746

146. C.F. Wen, M. Zhou, P.F. Liu, Y. Liu, X. Wu et al., Highly ethylene-selective electrocatalytic CO_2 reduction enabled by isolated Cu-S motifs in metal-organic framework based precatalysts. Angew. Chem. Int. Ed. **61**(2), e202111700 (2022). https://doi.org/10.1002/anie.202111700

147. X.-F. Qiu, H.-L. Zhu, J.-R. Huang, P.-Q. Liao, X.-M. Chen, Highly selective CO_2 electroreduction to C_2H_4 using a metal-organic framework with dual active sites. J. Am. Chem. Soc. **143**(19), 7242–7246 (2021). https://doi.org/10.1021/jacs.1c01466

148. L.-L. Zhuo, P. Chen, K. Zheng, X.-W. Zhang, J.-X. Wu et al., Flexible cuprous triazolate frameworks as highly stable and efficient electrocatalysts for CO_2 reduction with tunable C_2H_4/CH_4 selectivity. Angew. Chem. Int. Ed. **61**(28), e202204967 (2022). https://doi.org/10.1002/anie.202204967

149. J. Gao, D. Ren, X.Y. Guo, S.M. Zakeeruddin, M. Gratzel, Sequential catalysis enables enhanced C–C coupling towards multi-carbon alkenes and alcohols in carbon dioxide reduction: a study on bifunctional Cu/Au electrocatalysts. Faraday Discuss **215**, 282–296 (2019). https://doi.org/10.1039/c8fd00219c

150. J. Gao, H. Zhang, X.Y. Guo, J.S. Luo, S.M. Zakeeruddin et al., Selective C–C coupling in carbon dioxide electroreduction via efficient spillover of intermediates as supported by operando raman spectroscopy. J. Am. Chem. Soc. **141**(47), 18704–18714 (2019). https://doi.org/10.1021/jacs.9b07415

151. D. Ren, B.S.H. Ang, B.S. Yeo, Tuning the selectivity of carbon dioxide electroreduction toward ethanol on oxide-derived Cu_xZn catalysts. ACS Catal. **6**(12), 8239–8247 (2016). https://doi.org/10.1021/acscatal.6b02162

152. X.S. Su, Y.M. Sun, L. Jin, L. Zhang, Y. Yang et al., Hierarchically porous Cu/Zn bimetallic catalysts for highly selective CO_2 electroreduction to liquid C_2 products. Appl. Catal. B-Environ. **269**, 118800 (2020). https://doi.org/10.1016/j.apcatb.2020.118800

153. A. Dutta, I.Z. Montiel, R. Erni, K. Kiran, M. Rahaman et al., Activation of bimetallic AgCu foam electrocatalysts for ethanol formation from CO_2 by selective Cu oxidation/reduction. Nano Energy **68**, 104331 (2020). https://doi.org/10.1016/j.nanoen.2019.104331

154. T.T.H. Hoang, S. Verma, S.C. Ma, T.T. Fister, J. Timoshenko et al., Nanoporous copper silver alloys by additive-controlled electrodeposition for the selective electroreduction of CO_2 to

ethylene and ethanol. J. Am. Chem. Soc. **140**(17), 5791–5797 (2018). https://doi.org/10.1021/jacs.8b01868

155. Z. Yin, J. Yu, Z. Xie, S.-W. Yu, L. Zhang et al., Hybrid catalyst coupling single-atom ni and nanoscale Cu for efficient CO_2 electroreduction to ethylene. J. Am. Chem. Soc. **144**(45), 20931–20938 (2022). https://doi.org/10.1021/jacs.2c09773

156. Y.B. Ma, J.L. Yu, M.Z. Sun, B. Chen, X.C. Zhou et al., Confined growth of silver-copper janus nanostructures with 100 facets for highly selective tandem electrocatalytic carbon dioxide reduction. Adv. Mater. **34**(19), 2110607 (2022). https://doi.org/10.1002/adma.202110607

157. M. Hirsimaki, M. Lampimaki, K. Lahtonen, I. Chorkendoff, M. Valden, Investigation of the role of oxygen induced segregation of Cu during Cu_2O formation on Cu{100}, Ag/Cu{100} and Cu(Ag) alloy. Surf. Sci. **583**(2–3), 157–165 (2005). https://doi.org/10.1016/j.susc.2005.03.035

158. J. Choi, M.J. Kim, S.H. Ahn, I. Choi, J.H. Jang et al., Electrochemical CO_2 reduction to CO on dendritic Ag-Cu electrocatalysts prepared by electrodeposition. Chem. Eng. J. **299**, 37–44 (2016). https://doi.org/10.1016/j.cej.2016.04.037

159. J.Q. Wang, Z. Li, C.K. Dong, Y. Feng, J. Yang et al., Silver/copper interface for relay electroreduction of carbon dioxide to ethylene. ACS Appl. Mater. Interfaces **11**(3), 2763–2767 (2019). https://doi.org/10.1021/acsami.8b20545

160. J.F. Huang, M. Mensi, E. Oveisi, V. Mantella, R. Buonsanti, Structural sensitivities in bimetallic catalysts for electrochemical CO_2 reduction revealed by Ag-Cu nanodimers. J. Am. Chem. Soc. **141**(6), 2490–2499 (2019). https://doi.org/10.1021/jacs.8b12381

161. Y. Feng, Z. Li, H. Liu, C.K. Dong, J.Q. Wang et al., Laser-prepared cuzn alloy catalyst for selective electrochemical reduction of CO_2 to ethylene. Langmuir **34**(45), 13544–13549 (2018). https://doi.org/10.1021/acs.langmuir.8b02837

162. S. Ma, M. Sadakiyo, M. Heima, R. Luo, R.T. Haasch et al., Electroreduction of carbon dioxide to hydrocarbons using bimetallic Cu-Pd catalysts with different mixing patterns. J. Am. Chem. Soc. **139**(1), 47–50 (2017). https://doi.org/10.1021/jacs.6b10740

163. L.K. Xiong, X. Zhang, H. Yuan, J. Wang, X.Z. Yuan et al., Breaking the linear scaling relationship by compositional and structural crafting of ternary Cu-Au/Ag nanoframes for electrocatalytic ethylene production. Angew. Chem. Int. Ed. **60**(5), 2508–2518 (2021). https://doi.org/10.1002/anie.202012631

164. Q.C. Wang, Y.P. Lei, D.S. Wang, Y.D. Li, Defect engineering in earth-abundant electrocatalysts for CO_2 and N_2 reduction. Energy Environ. Sci. **12**(6), 1730–1750 (2019). https://doi.org/10.1039/c8ee03781g

165. Y.F. Wang, P. Han, X.M. Lv, L.J. Zhang, G.F. Zheng, Defect and interface engineering for aqueous electrocatalytic CO_2 reduction. Joule **2**(12), 2551–2582 (2018). https://doi.org/10.1016/j.joule.2018.09.021

166. H.S. Jeon, S. Kunze, F. Scholten, B. Roldan Cuenya, Prism-shaped Cu nanocatalysts for electrochemical CO_2 reduction to ethylene. ACS Catal. **8**(1), 531–535 (2018). https://doi.org/10.1021/acscatal.7b02959

167. K.D. Yang, W.R. Ko, J.H. Lee, S.J. Kim, H. Lee et al., Morphology-directed selective production of ethylene or ethane from CO_2 on a Cu mesopore electrode. Angew. Chem. Int. Ed. **56**(3), 796–800 (2017). https://doi.org/10.1002/anie.201610432

168. Y.W. Jiang, X.Y. Wang, D.L. Duan, C.H. He, J. Ma et al., Structural reconstruction of cu2o superparticles toward electrocatalytic CO_2 reduction with high C_{2+} products selectivity. Adv. Sci. **9**, 2105292 (2022). https://doi.org/10.1002/advs.202105292

169. Z.X. Gu, N. Yang, P. Han, M. Kuang, B.B. Mei et al., Oxygen vacancy tuning toward efficient electrocatalytic CO_2 reduction to C_2H_4. Small Methods **3**(2), 1800449 (2019). https://doi.org/10.1002/smtd.201800449

170. X. Liu, X. Wang, B. Zhou, W.-C. Law, A.N. Cartwright et al., Size-controlled synthesis of $Cu_{2-x}E$ (E = S, Se) nanocrystals with strong tunable near-infrared localized surface plasmon resonance and high conductivity in thin films. Adv. Funct. Mater. **23**(10), 1256–1264 (2013). https://doi.org/10.1002/adfm.201202061

171. J.M. Luther, P.K. Jain, T. Ewers, A.P. Alivisatos, Localized surface plasmon resonances arising from free carriers in doped quantum dots. Nat. Mater. **10**(5), 361–366 (2011). https://doi.org/10.1038/nmat3004

172. T.-T. Zhuang, Z.-Q. Liang, A. Seifitokaldani, Y. Li, P. De Luna et al., Steering post-C–C coupling selectivity enables high efficiency electroreduction of carbon dioxide to multi-carbon alcohols. Nat. Catal. **1**(6), 421–428 (2018). https://doi.org/10.1038/s41929-018-0084-7

173. I. Kasatkin, P. Kurr, B. Kniep, A. Trunschke, R. Schlögl, Role of lattice strain and defects in copper particles on the activity of $Cu/ZnO/Al_2O_3$ catalysts for methanol synthesis. Angew. Chem. Int. Ed. **46**(38), 7324–7327 (2007). https://doi.org/10.1002/anie.200702600

174. T.-N. Ye, S.-W. Park, Y. Lu, J. Li, M. Sasase et al., Vacancy-enabled N_2 activation for ammonia synthesis on an Ni-loaded catalyst. Nature **583**(7816), 391–395 (2020). https://doi.org/10.1038/s41586-020-2464-9

175. Y. Jing, S. Huang, J. Wu, M. Meng, X. Li et al., A single-electron transistor made of a 3d topological insulator nanoplate. Adv. Mater. **31**(42), 1903686 (2019). https://doi.org/10.1002/adma.201903686

176. C. Peng, G. Luo, Z. Xu, S. Yan, J. Zhang et al., Lithiation-enabled high-density nitrogen vacancies electrocatalyze CO_2 to C_2 products. Adv. Mater. **33**(40), 2103150 (2021). https://doi.org/10.1002/adma.202103150

177. H. Xu, L. Chen, J. Shi, Advanced electrocatalytic systems for enhanced atom/electron utilization. Energy Environ. Sci. **16**(4), 1334–1363 (2023). https://doi.org/10.1039/D2EE03323B

178. Z.Y. Yin, C. Yu, Z.L. Zhao, X.F. Guo, M.Q. Shen et al., Cu_3N nanocubes for selective electrochemical reduction of CO_2 to ethylene. Nano Lett. **19**(12), 8658–8663 (2019). https://doi.org/10.1021/acs.nanolett.9b03324

179. Y.Y. Mi, X.Y. Peng, X.J. Liu, J. Luo, Selective formation of C2 products from electrochemical CO_2 reduction over

Cu$_{1.8}$Se nanowires. ACS Appl. Energy Mater. **1**(10), 5119–5123 (2018). https://doi.org/10.1021/acsaem.8b00744

180. J. Li, A. Ozden, M.Y. Wan, Y.F. Hu, F.W. Li et al., Silica-copper catalyst interfaces enable carbon-carbon coupling towards ethylene electrosynthesis. Nat. Commun. **12**(1), 2808 (2021). https://doi.org/10.1038/s41467-021-23023-0

181. F.P.G. de Arquer, C.T. Dinh, A. Ozden, J. Wicks, C. McCallum et al., CO$_2$ electrolysis to multicarbon products at activities greater than 1 A cm^{-2}. Science **367**(6478), 661–666 (2020). https://doi.org/10.1126/science.aay4217

182. H.Q. Liang, S. Zhao, X.M. Hu, M. Ceccato, T. Skrydstrup et al., Hydrophobic copper interfaces boost electroreduction of carbon dioxide to ethylene in water. ACS Catal. **11**(2), 958–966 (2021). https://doi.org/10.1021/acscatal.0c03766

183. R.X. Chen, H.Y. Su, D.Y. Liu, R. Huang, X.G. Meng et al., Highly selective production of ethylene by the electroreduction of carbon monoxide. Angew. Chem. Int. Ed. **59**(1), 154–160 (2020). https://doi.org/10.1002/anie.201910662

184. X. Wei, Z.L. Yin, K.J. Lyu, Z. Li, J. Gong et al., Highly selective reduction of CO$_2$ to C$_{2+}$ hydrocarbons at copper/polyaniline interfaces. ACS Catal. **10**(7), 4103–4111 (2020). https://doi.org/10.1021/acscatal.0c00049

185. A. Thevenon, A. Rosas-Hernandez, J.C. Peters, T. Agapie, In-situ nanostructuring and stabilization of polycrystalline copper by an organic salt additive promotes electrocatalytic CO$_2$ reduction to ethylene. Angew. Chem. Int. Ed. **58**(47), 16952–16958 (2019). https://doi.org/10.1002/anie.201907935

186. X.Y. Chen, J.F. Chen, N.M. Alghoraibi, D.A. Henckel, R.X. Zhang et al., Electrochemical CO$_2$-to-ethylene conversion on polyamine-incorporated Cu electrodes. Nat. Catal. **4**(1), 20–27 (2021). https://doi.org/10.1038/s41929-020-00547-0

187. L. Yuan, L. Zhang, J. Feng, C. Jiang, J. Feng et al., Upscaling studies for efficiently electric-driven CO$_2$ reduction to CO in ionic liquid-based electrolytes. Chem. Eng. J. **450**, 138378 (2022). https://doi.org/10.1016/j.cej.2022.138378

188. Y. Wang, W. Wang, J. Xie, C.-H. Wang, Y.-W. Yang et al., Electrochemical reduction of CO$_2$ in ionic liquid: Mechanistic study of Li-CO$_2$ batteries via in situ ambient pressure x-ray photoelectron spectroscopy. Nano Energy **83**, 105830 (2021). https://doi.org/10.1016/j.nanoen.2021.105830

189. Y.F. Sha, J.L. Zhang, X.Y. Cheng, M.Z. Xu, Z.Z. Su et al., Anchoring ionic liquid in copper electrocatalyst for improving CO$_2$ conversion to ethylene. Angew. Chem. Int. Ed. **61**, 13 (2022). https://doi.org/10.1002/anie.202200039

190. C.L. Xiao, J. Zhang, Architectural design for enhanced C$_2$ product selectivity in electrochemical CO$_2$ reduction using Cu-based catalysts: a review. ACS Nano **15**(5), 7975–8000 (2021). https://doi.org/10.1021/acsnano.0c10697

191. J. Wang, H.-Y. Tan, Y. Zhu, H. Chu, H.M. Chen, Linking the dynamic chemical state of catalysts with the product profile of electrocatalytic CO$_2$ reduction. Angew. Chem. Int. Ed. **60**(32), 17254–17267 (2021). https://doi.org/10.1002/anie.202017181

192. P.P. Yang, X.L. Zhang, F.Y. Gao, Y.R. Zheng, Z.Z. Niu et al., Protecting copper oxidation state via intermediate confinement for selective CO$_2$ electroreduction to C$_{2+}$ fuels. J. Am. Chem. Soc. **142**(13), 6400–6408 (2020). https://doi.org/10.1021/jacs.0c01699

193. H. Xiao, W.A. Goddard, T. Cheng, Y.Y. Liu, Cu metal embedded in oxidized matrix catalyst to promote CO$_2$ activation and CO dimerization for electrochemical reduction of CO$_2$. Proc. Natl. Acad. Sci. **114**(26), 6685–6688 (2017). https://doi.org/10.1073/pnas.1702405114

194. T.C. Chou, C.C. Chang, H.L. Yu, W.Y. Yu, C.L. Dong et al., Controlling the oxidation state of the Cu electrode and reaction intermediates for electrochemical CO$_2$ reduction to ethylene. J. Am. Chem. Soc. **142**(6), 2857–2867 (2020). https://doi.org/10.1021/jacs.9b11126

195. P. De Luna, R. Quintero-Bermudez, C.T. Dinh, M.B. Ross, O.S. Bushuyev et al., Catalyst electro-redeposition controls morphology and oxidation state for selective carbon dioxide reduction. Nat. Catal. **1**(2), 103–110 (2018). https://doi.org/10.1038/s41929-017-0018-9

196. X. Yuan, S. Chen, D. Cheng, L. Li, W. Zhu et al., Controllable Cu^0-Cu$^+$ sites for electrocatalytic reduction of carbon dioxide. Angew. Chem. Int. Ed. **60**(28), 15344–15347 (2021). https://doi.org/10.1002/anie.202105118

197. X. Li, Q. Liu, J. Wang, D. Meng, Y. Shu et al., Enhanced electroreduction of CO$_2$ to C$_{2+}$ products on heterostructured Cu/oxide electrodes. Chem **8**(8), 2148–2162 (2022). https://doi.org/10.1016/j.chempr.2022.04.004

198. D. Gao, I. Sinev, F. Scholten, R.M. Arán-Ais, N.J. Divins et al., Selective CO$_2$ electroreduction to ethylene and multicarbon alcohols via electrolyte-driven nanostructuring. Angew. Chem. Int. Ed. **131**(47), 17203–17209 (2019). https://doi.org/10.1002/anie.201910155

199. W. Zhang, C. Huang, Q. Xiao, L. Yu, L. Shuai et al., Atypical oxygen-bearing copper boosts ethylene selectivity toward electrocatalytic CO$_2$ reduction. J. Am. Chem. Soc. **142**(26), 11417–11427 (2020). https://doi.org/10.1021/jacs.0c01562

200. H. Sun, L. Chen, L. Xiong, K. Feng, Y. Chen et al., Promoting ethylene production over a wide potential window on Cu crystallites induced and stabilized via current shock and charge delocalization. Nat. Commun. **12**(1), 6823 (2021). https://doi.org/10.1038/s41467-021-27169-9

201. S. Sultan, H. Lee, S. Park, M.M. Kim, A. Yoon et al., Interface rich CuO/Al$_2$CuO$_4$ surface for selective ethylene production from electrochemical CO$_2$ conversion. Energy Environ. Sci. **15**(6), 2397–2409 (2022). https://doi.org/10.1039/D1EE03861C

202. A. Guan, Z. Chen, Y. Quan, C. Peng, Z. Wang et al., Boosting CO$_2$ electroreduction to CH$_4$ via tuning neighboring single-copper sites. ACS Energy Lett. **5**(4), 1044–1053 (2020). https://doi.org/10.1021/acsenergylett.0c00018

203. P. Shao, H.X. Zhang, Q.L. Hong, L. Yi, Q.H. Li et al., Enhancing CO$_2$ electroreduction to ethylene via copper-silver tandem catalyst in boron-imidazolate framework nanosheet. Adv. Energy Mater. **13**(19), 2300088 (2023). https://doi.org/10.1002/aenm.202300088

204. A. Ozden, F. Li, F.P. Garciá de Arquer, A. Rosas-Hernández, A. Thevenon et al., High-rate and efficient ethylene electrosynthesis using a catalyst/promoter/transport layer. ACS Energy Lett. **5**(9), 2811–2818 (2020). https://doi.org/10.1021/acsenergylett.0c01266

205. R. Wang, J. Liu, Q. Huang, L.Z. Dong, S.L. Li et al., Partial coordination-perturbed bi-copper sites for selective electroreduction of CO_2 to hydrocarbons. Angew. Chem. Int. Ed. **60**(36), 19829–19835 (2021). https://doi.org/10.1002/anie.202105343

206. M. Balamurugan, H.Y. Jeong, V.S.K. Choutipalli, J.S. Hong, H. Seo et al., Electrocatalytic reduction of CO_2 to ethylene by molecular Cu-complex immobilized on graphitized mesoporous carbon. Small **16**(25), 2000955 (2020). https://doi.org/10.1002/smll.202000955

207. X. Xie, X. Zhang, M. Xie, L. Xiong, H. Sun et al., Au-activated N motifs in non-coherent cupric porphyrin metal organic frameworks for promoting and stabilizing ethylene production. Nat. Commun. **13**(1), 63 (2022). https://doi.org/10.1038/s41467-021-27768-6

208. Y.-R. Lin, D.U. Lee, S. Tan, D.M. Koshy, T.Y. Lin et al., Vapor-fed electrolyzers for carbon dioxide reduction using tandem electrocatalysts: cuprous oxide coupled with nickel-coordinated nitrogen-doped carbon. Adv. Funct. Mater. **32**(28), 2113252 (2022). https://doi.org/10.1002/adfm.202113252

209. W.H. Lee, C. Lim, S.Y. Lee, K.H. Chae, C.H. Choi et al., Highly selective and stackable electrode design for gaseous CO_2 electroreduction to ethylene in a zero-gap configuration. Nano Energy **84**, 105859 (2021). https://doi.org/10.1016/j.nanoen.2021.105859

210. A. Ozden, Y. Wang, F. Li, M. Luo, J. Sisler et al., Cascade CO_2 electroreduction enables efficient carbonate-free production of ethylene. Joule **5**(3), 706–719 (2021). https://doi.org/10.1016/j.joule.2021.01.007

211. Y.N. Xu, W. Li, H.Q. Fu, X.Y. Zhang, J.Y. Zhao et al., Tuning the microenvironment in monolayer mgal layered double hydroxide for CO_2-to-ethylene electrocatalysis in neutral media. Angew. Chem. Int. Ed. **135**(19), 2217296 (2023). https://doi.org/10.1002/ange.202217296

212. Y. Zhou, F. Che, M. Liu, C. Zou, Z. Liang et al., Dopant-induced electron localization drives CO_2 reduction to C_2 hydrocarbons. Nat. Chem. **10**(9), 974–980 (2018). https://doi.org/10.1038/s41557-018-0092-x

213. S.Y. Lee, H. Jung, N.-K. Kim, H.-S. Oh, B.K. Min et al., Mixed copper states in anodized Cu electrocatalyst for stable and selective ethylene production from CO_2 reduction. J. Am. Chem. Soc. **140**(28), 8681–8689 (2018). https://doi.org/10.1021/jacs.8b02173

214. H. Mistry, A.S. Varela, C.S. Bonifacio, I. Zegkinoglou, I. Sinev et al., Highly selective plasma-activated copper catalysts for carbon dioxide reduction to ethylene. Nat. Commun. **7**(1), 12123 (2016). https://doi.org/10.1038/ncomms12123

215. H. Chen, Z. Wang, X. Wei, S. Liu, P. Guo et al., Promotion of electrochemical CO_2 reduction to ethylene on phosphorus-doped copper nanocrystals with stable $Cu^{\delta+}$ sites. Appl. Surf. Sci. **544**, 148965 (2021). https://doi.org/10.1016/j.apsusc.2021.148965

216. H. Li, T. Liu, P. Wei, L. Lin, D. Gao et al., High-rate CO_2 electroreduction to C_{2+} products over a copper-copper iodide catalyst. Angew. Chem. Int. Ed. **133**(26), 14450–14454 (2021). https://doi.org/10.1002/ange.202102657

217. A. Vasileff, C. Xu, Y. Jiao, Y. Zheng, S.-Z. Qiao, Surface and interface engineering in copper-based bimetallic materials for selective CO_2 electroreduction. Chem **4**(8), 1809–1831 (2018). https://doi.org/10.1016/j.chempr.2018.05.001

218. D. Kim, J. Resasco, Y. Yu, A.M. Asiri, P. Yang, Synergistic geometric and electronic effects for electrochemical reduction of carbon dioxide using gold-copper bimetallic nanoparticles. Nat. Commun. **5**, 4948 (2014). https://doi.org/10.1038/ncomms5948

219. S. Popović, M. Smiljanić, P. Jovanovič, J. Vavra, R. Buonsanti et al., Stability and degradation mechanisms of copper-based catalysts for electrochemical CO_2 reduction. Angew. Chem. Int. Ed. **59**(35), 14736–14746 (2020). https://doi.org/10.1002/anie.202000617

220. S.H. Lee, J.C. Lin, M. Farmand, A.T. Landers, J.T. Feaster et al., Oxidation state and surface reconstruction of Cu under CO_2 reduction conditions from in situ X-ray characterization. J. Am. Chem. Soc. **143**(2), 588–592 (2021). https://doi.org/10.1021/jacs.0c10017

221. T. Burdyny, W.A. Smith, CO_2 reduction on gas-diffusion electrodes and why catalytic performance must be assessed at commercially-relevant conditions. Energy Environ. Sci. **12**(5), 1442–1453 (2019). https://doi.org/10.1039/C8EE03134G

222. Y. Luo, K. Zhang, Y. Li, Y. Wang, Valorizing carbon dioxide via electrochemical reduction on gas-diffusion electrodes. InfoMat **3**(12), 1313–1332 (2021). https://doi.org/10.1002/inf2.12253

223. Q. Gong, P. Ding, M. Xu, X. Zhu, M. Wang et al., Structural defects on converted bismuth oxide nanotubes enable highly active electrocatalysis of carbon dioxide reduction. Nat. Commun. **10**(1), 1–10 (2019). https://doi.org/10.1038/s41467-019-10819-4

224. J.Y.T. Kim, P. Zhu, F.-Y. Chen, Z.-Y. Wu, D.A. Cullen et al., Recovering carbon losses in CO_2 electrolysis using a solid electrolyte reactor. Nat. Catal. **5**(4), 288–299 (2022). https://doi.org/10.1038/s41929-022-00763-w

225. W. Luc, B.H. Ko, S. Kattel, S. Li, D. Su et al., SO_2-induced selectivity change in CO_2 electroreduction. J. Am. Chem. Soc. **141**(25), 9902–9909 (2019). https://doi.org/10.1021/jacs.9b03215

226. C. Chen, X. Yan, S. Liu, Y. Wu, Q. Wan et al., Highly efficient electroreduction of CO_2 to C_{2+} alcohols on heterogeneous dual active sites. Angew. Chem. Int. Ed. **59**(38), 16459–16464 (2020). https://doi.org/10.1002/anie.202006847